Long-term eddy modulation inhibited the meridional asymmetry of halocline in the Beaufort Gyre

Jinling Lu[1,2], Ling Du[1,2], Shuhao Tao[1,2]

[1] Frontier Science Center for Deep Ocean Multispheres and Earth System (FDOMES) and Physical Oceanography Laboratory, Ocean University of China, Qingdao, 266100, China
[2] College of Oceanic and Atmospheric Sciences, Ocean University of China, Qingdao, 266100, China

Correspondence to: Ling Du (duling@ouc.edu.cn)

Abstract. Under the background of wind forcing change along with Arctic sea ice retreat, the mesoscale processes undergoing distinct variation in the Beaufort Gyre (BG) region are ~~more and more significant~~increasingly important to oceanic transport and energic cascade, and then these changes put oceanic stratification into a new state. Here, the varying number and strength of eddies ~~and eddy kinetic energy (EKE)~~ in the central Canada Basin (CB) and Chukchi–Beaufort continental slope are obtained based on mooring observations (2003–2018), altimetry measurements (1993–2019) and reanalysis data (1980–2021). In this paper, the variability ~~of~~in the BG halocline ~~in BG~~ representing the adjustment of stratification in the upper layer is shown ~~so as~~ to ~~analyze~~analyse how it occurs under ~~significantly~~ changing mesoscale processes. We find that the halocline depth has deepened by ~40 m in the south while that in the north has deepened by ~70 m in ~~the in the last~~ nearly the last two decades ~~by~~according to multiple ~~data sets~~datasets. The asymmetrical halocline ~~depth~~ lifting to the north initially ~~was~~ shifted to a final nearly ~~symmetric~~symmetrical structure. ~~Eddy strength and Eddy~~ In the meantime, eddy activities in the upper layer from the southern margin of BG to the abyssal plain have been enhanced. Moreover, eddy-induced low--salinity water transportations have been continuously increasing ~~toward~~towards the central basin ~~at the mean time the~~ as halocline ~~depth and strength among the southern and northern parts in the basin have reached~~structures on either side of the gyre reach a nearly identical and stable regime. It ~~is clearly~~was clarified that the long-term ~~dynamical~~dynamic eddy modulation through eddy fluxes facilitating the freshwater redistribution inhibited the meridional asymmetry of the BG halocline ~~of the BG~~. Further research into reconciling high-resolution observations and data simulations can ~~helps us to~~provide a better ~~understand~~understanding of the eddy modulation processes and ~~its~~their influence on large-scale circulation.

1 Introduction

Global temperatures have continued to rise since the 1970s. The Arctic Ocean, as the focal point of climate change research, is the region with the most dramatic global surface temperature warming (Huang et al., 2018), with ~~the~~a warming range as high as 1.2 °C/10a, more than twice the global average warming range, which is called the "Arctic amplification" phenomenon (Serreze and Barry, 2011). These variations not only affect the upper ocean circulation, but also expose the Arctic atmosphere–ice–sea system to rapid changes (Moore et al., 2018; Timmermans and Marshall, 2020). In this context, with summer sea ice

declining in the Arctic (Stroeve et al., 2007, 2014; Niederdrenk and Notz, 2018), the presence of increased freshwater in the upper layer alters local stratification, resulting in the variability of water masses. Meanwhile, increased active ocean–atmosphere interactions and mesoscale processes in the Canada Basin (CB) due to the emergence of broader open areas have attracted increasing attention.

The Beaufort Gyre (BG) in the CB, a large-scale wind-driven anticyclonic circulation feature, that stores a substantial amount of freshwater in the CB (Proshutinsky et al., 2009, 2019), is accompanied by prevalent mesoscale eddies (Doddridge et al., 2019; Manucharyan and Spall, 2016; Zhao and Timmermans 2015; Zhao et al. 2016). The halocline in the CB, a thick layer with a double peak of stratification, is considered an insulating "density barrier" between the surface mixed layer and the Atlantic water layer underneath (Bourgain and Gascard, 2011). The asymmetrical stratification of the BG and halocline vertical structure have received attention in recent studies (Kenigson et al., 2021; Zhang et al., 2023). The gyre is highly asymmetrical and associated with surface forcing and topography, with isohalines steeper in the south and east than in the north and west (Zhang et al., 2023). Isopycnals are also steeper near the gyre edge than the interior, indicating stronger baroclinic instability (Manucharyan et al., 2016). In addition, the freshwater content (FWC) accumulated by Ekman convergence increased between 2003 and 2008 and remained relatively constant between 2008 and 2012 (Timmermans and Toole, 2023). Pacific Winter Water (PWW), which lies above the eastern Arctic origin lower halocline water, is recognised as a component of the western Arctic halocline (Shimada et al., 2005). Observations indicated that the PWW layer generally deepened during 2004–2018 while isopycnal layer thickness increased (Kenigson et al., 2021). Likewise, there was an isopycnal deepening by 70 m during 2004–2011 (Zhong et al., 2018), suggesting a spin-up of the gyre. The isopycnal slope is increasing with depth, which can be attributed to the eddy-induced stream function, explaining the increased PWW thickness in the interior (Kenigson et al., 2021).

Previous works on eddies in the CB or the Arctic Ocean were mostly based on satellite products (e.g., Kozlov et al., 2019; Kubryakov et al., 2021, Raj et al., 2016), in situ hydrographic data (e.g., Fer et al., 2018; Timmermans et al., 2008; Zhao et al., 2014, 2016; Zhao and Timmermans, 2015), and high-resolution, eddy-resolving simulations (e.g., Reagan et al., 2020; Wang et al., 2020). Eddy activity, a common feature in the BG halocline, has also been the focus of many past studies. Moreover, the kinetic energy of BG mesoscale eddy activities is dominant in the BG halocline (Zhao et al., 2016, 2018). Eddies are mainly concentrated in the subsurface (30–300 m) even though they can extend to thousands of metres in depth (Zhao et al., 2014; Zhao and Timmermans, 2015), due to eddy dissipation by ice–ocean drag in the surface boundary layer (Manucharyan and Stewart, 2022). The depth of EKE maximum value is generally found at approximately 70–110 m in the halocline (Wang et al., 2020). Based on 127 eddies observed at drifting sea ice stations, Manley

65 and Hunkins (1985) found that the eddy kinetic energy (EKE) accounted for approximately one-third of the total kinetic energy of the upper 200 m in the CB.

From the perspective of horizontal patterns, the southern CB is popular with a large number of cold-core and anticyclonic halocline eddies (Spall et al., 2008). Zhao et al. (2016) kept Ice Tethered Profiler (ITP)
70 measurements for temperature, salinity, and current between 2005 and 2015 to survey the changes in the eddy field in the CB. They found that eddies were mostly distributed in the western and southern parts of the CB. EKE derived by satellites is also higher along the major boundary currents and continental shelves in the Arctic Ocean (Timmermans and Marshall 2020; Wang et al., 2020).

The number of eddies in the lower halocline doubled from 2005–2012 to 2013–2014 (Zhao et al., 2016), with the past
75 increase in FWC, gyre areas, and strength (Regan et al., 2019; Timmermans and Toole, 2023; Zhang et al., 2016). The response of EKE to the spin-up of the gyre during 2003–2007 showed that EKE at the subsurface has generally strengthened (Regan et al., 2020). Recent research has also demonstrated that with wind energy input increasing into the BG due to the significant loss of sea ice after 2007, eddy activities would also be more active (Armitage et al., 2020).
80 Mesoscale eddies can transmit momentum, heat, water masses, and chemical compositions, not only contributing to atmospheric circulation, mass distribution, and marine biology but also playing an important role in global ocean heat balance (Chelton et al., 2007). Eddies not only exhibit unprecedented changes but also play a crucial role in the Ekman-driven BG stability in the context of sea ice loss (Manucharyan et al., 2016). They can balance atmosphere–ocean and ice–sea stress input, gradually weaken the isopycnal slope and geostrophic currents and counteract the
85 accumulation of FWC driven by Ekman pumping by dissipating available potential energy (APE). Eddy activity, as a key physical process, affects freshwater release and accumulation, and ultimately influences halocline formation (Manucharyan and Spall, 2016). In addition, Ekman pumping and sea ice are also major factors affecting halocline dynamics. This balance between halocline and eddies is thought to occur on different time scales in realistic models, which suggests a link between small-scale features and changes to
90 large-scale circulation (Doddridge et al., 2019; Manucharyan et al., 2017).

However, with sea ice conditions changing due to global warming, the long-term variability of eddies in the central basin and basin boundary regions is still unsolved. Furthermore, according to the standpoint about possible gyre stabilisation in recent years (Proshutinsky et al., 2019; Zhang et al., 2016), the eddy modulation in the BG halocline on a long timescale is still unknown. Due to influence of the measurement conditions and limited satellite
95 observations, continuous eddy observation data in space and time are relatively scarce. Data coverage in space and time has yet to be improved (Zhao et al., 2016). The results of numerical simulations lack effective data to support them, so research on oceanic mesoscale eddies remains uncertain to some extent. Here, we use multiple datasets containing moored, in situ, and satellite altimetry observations, in comparison with reanalysis data,

to quantify the strength of mesoscale processes by ~~sea level anomaly (~~SLA~~)~~ and ~~horizonal~~horizontal currents. The stationary eddies and EKE~~.~~, as well as the transformation of ~~the~~ halocline structure across the basin~~.~~, are both ~~pointed out~~noted to assess the low~~-~~-frequency variability of ~~the~~ halocline in ~~the~~ BG under ~~significantly~~ the changing ~~mesoscale eddies.~~eddy modulation. Section 2 presents the details of ~~the~~ data and methodology. Section 3 demonstrates the halocline variability~~,~~ especially on its meridional asymmetry in the BG region. ~~And~~The eddy distribution and ~~interannual~~long-term changes are discussed in ~~Section~~section 4. Section 5 explains significant eddy modulation in the halocline structures as well as the correlation ~~of~~between EKE and geostrophic currents ~~as well significant eddy modulation in the halocline.~~. Section 6 is ~~the~~ summary and discussion ~~in~~of this paper.

2 Data and methods

2.1 Observations and ocean reanalysis data

In this paper~~,~~ we ~~used~~use multiple ~~data sets~~datasets, including hydrographic observations, satellite altimetry~~,~~ and reanalysis ~~data sets~~datasets. The hydrographic data are in situ measurements from ~~Conductivity Temperature Depth (~~CTD~~)~~ and mooring ~~data~~observation from McLane Moored Profilers (MMPs) at four moorings that are all deployed under the Beaufort Gyre Exploration Project (BGEP, http://www.whoi.edu/beaufortgyre/data). The reanalysis ~~data sets~~datasets used here mainly ~~consists~~consist of World Ocean Atlas ~~2018 (WOA18~~2023 (WOA23) and Simple Ocean Data Assimilation (SODA, version 3.4.2).

~~Annual~~An annual hydrographic survey through ship~~-~~-based CTD has been conducted in the BG region each year between August and October. CTD data between 2004 and 2021 are mainly used to ~~mainly~~ investigate ~~spatio-temporal~~the spatiotemporal variability ~~of~~in oceanic stratification across the ~~CB.~~fundamental BG region (Fig. 1a). The positions of the deployed CTD instruments ~~deployed is~~are shown in Fig. ~~1a. Plus~~1b. Additionally, to supplement the long-term trends and changing characteristics of the halocline and to capture mesoscale eddies at representative stations in the CB, mooring data deployed at four corners around the basin (Fig. ~~1b~~1c) between mid~~-~~-2003 and mid~~-~~-2018 above 500 m are also ~~analyzed~~analysed. Each mooring system included a MMP that ~~returned~~returns profiles of horizontal velocity, temperature, salinity, pressure~~ and~~, etc. A pair of upgoing/downgoing profiles (separated by 6 hours) ~~was~~is returned every other day, and the data ~~were~~are processed to a vertical resolution of 2 dbar. The shallowest moored measurement varies from ~~about~~approximately 50–90 m (depending on the mooring and sampling period) to avoid collisions with ice keels~~,~~ and the deepest measurements are~~ to~~ 2000 m.
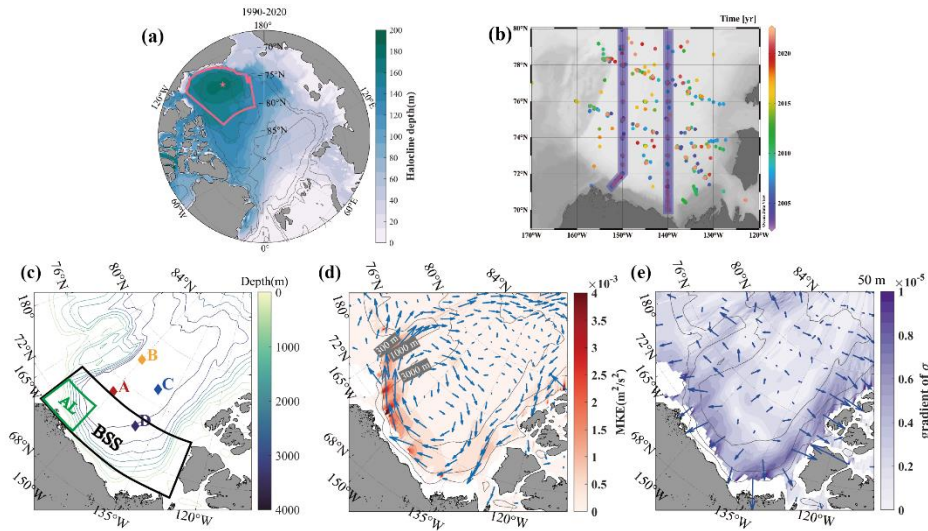
Figure 1. (a) <u>A map of climatology halocline depth. Pink box and star indicate the BG area and centre, referring to Regan et al. (2020). This BG box is defined as the region between 70.5–80.5°N and 170–130°W, bounded by the 300 m bathymetry. The centre of the mean gyre from 1990 to 2014 is situated at 74.74°N and 150.62°W. (b)</u>The positions of in situ sites of CTD measurement from BGEP in ~~a~~ certain months during 2004–2021. The purple ~~bar indicates an artificially selected~~<u>bars indicate two</u> meridional ~~transect~~<u>transects</u> with a width of ~~36km~~<u>36 km</u> mostly along 150°W ~~but partially bent at the southwestern continental slope in Beaufort Sea. (b~~<u>and 140°W. (c</u>) A map of the Canada Basin and the bathymetric contours ~~upper than~~<u>above the</u> 4000 m isobath. Coloured diamonds denote the locations of four BGEP moorings. The two chosen regions are shown by green (AL, Alaskan coast) and black (BSS, Beaufort Sea slope) boxes ~~respectively. (c~~ <u>(d</u>) The distribution of mean kinetic energy <u>(MKE)</u> at 50 m. Vectors denote the ~~directions~~<u>direction</u> of mean currents. ~~Gray~~<u>Grey</u> lines denote the 300 m, 1000 m<u>,</u> and 3000 m bathymetry. (d) The distribution of horizontal gradient of potential density (shading ~~and vector~~) at 50 m. Vectors point in the ~~directions~~<u>direction</u> of increasing potential density. The results of (~~c~~<u>a), (d), and (~~d~~<u>e</u>) are calculated from the ~~2005–2017~~<u>1990–2020</u> WOA climatology.

The SODA reanalysis ~~data set~~ is developed by the University of Maryland based on the Global Simple Ocean Data Assimilation System, which ~~adopted in this paper~~ is the 5-~~days averaged~~<u>day average</u> from 1980 to 2021 <u>adopted in this paper</u>, with a horizontal resolution of $1/2°\times1/2°$ and vertically divided into 50 layers with unequal spacing. We ~~obtained the~~<u>obtain</u> gridded altimetry data (product identifier: SEALEVEL_GLO_PHY_L4_REP_OBSERVATIONS_088_047) over the years ~~in the~~ 1993–2019 ~~period~~ from the Copernicus Marine Environmental Monitoring Service (CMEMS). This product consists of daily gridded maps of dynamic topography in ice-free regions that have been derived as a sum of mapped ~~sea level anomalies (SLA)~~<u>SLAs</u> calculated from combined measurements by different satellites and mean dynamic topography (MDT~~).~~<u>)</u> <u>(Kubryakov et al. 2021).</u>

2.2 Methods

~~For estimating~~<u>To estimate</u> EKE ~~to~~<u>and</u> assess the strength of eddy activities, we ~~used~~<u>use</u> ocean current data from ~~and~~ SODA and altimetry. Geostrophic velocities are calculated from sea level ~~hight~~<u>height</u>. The horizontal velocity is

5

~~decomposed~~deconstructed into annual mean velocity $(\bar{u}, \bar{v})$ and ~~abnormal value~~anomaly (u', v') (Penduff et al., 2004; Rieck et al., 2015, 2018; Regan et al., 2020):

$$u = \bar{u} + u', u = \bar{v} + v',$$

$$and\ then\ EKE = (u'^2 + v'^2)/2. \tag{1}$$

155 Note that the EKE in this paper is estimated by a low-frequency ''eddy'', which is defined as a departure from a long-term temporal mean, with a period (~~it depends~~depending on the temporal resolution of the data) of greater than 5 days or 1 day (Lucke et al., 2017). In addition, the vertical velocity shear $\partial U/\partial z$ can be related to the large-scale density field by the thermal wind relation ~~(Meneghello et al., 2021)~~

$$\frac{\partial U}{\partial z} = \frac{g}{f_o \rho_o} \frac{\partial \rho}{\partial z} \vec{k} \times \nabla z_\rho = \frac{N^2}{f_o} \vec{k} \times \nabla z_\rho \tag{2}$$

160 where **U** is the horizontal current field, N is the Brunt-Väisälä buoyancy frequency, which represents oceanic stratification, $\nabla z_\rho = (-\frac{\partial \rho}{\partial x}/\frac{\partial \rho}{\partial z}, -\frac{\partial \rho}{\partial y}/\frac{\partial \rho}{\partial z})$ is the isopycnal slope, ρ is the potential density of ~~sea water~~seawater, ρ_o is the average density of seawater, g is the gravity acceleration, and z is depth. (Meneghello et al., 2021). Developed by ~~(3~~Eq. (2), the horizontal velocity field is calculated by ~~the~~integration with depth from bottom to surface. ~~The~~As maps of the horizontal velocity field (Fig. ~~1c~~1d) and density gradient (Fig. ~~1d~~1e) at 50 m in the CB ~~are shown~~show, the main circulation feature is ~~clearly~~discerned, and the

165 southwestern basin near continental slopes is the key region for varying currents tending towards high EKE and instability. ~~For investigating~~To investigate the variation ~~of~~in the halocline ~~to~~and understand the shifting of oceanic stratification, we consider the depth of the potential density surface σ=27.4 (25) kg·m^{-3} to approximately represent the base (top) of the halocline (Timmermans et al., 2020). Based on the upper and lower boundary of the halocline, APE is defined as the amount of potential energy in a stratified fluid available for mixing and conversion into kinetic energy (Huang 1998; Munk and Wunsch 1998~~)~~).

170 The calculation of APE here is following Eq. (3~~) (Polyakov et al., 2018; Bertosio et al., 2022, partial modification):~~):

$$APE = \int_{z_2}^{z_1} g[\rho(z) - \rho_{ref}]z dz, \qquad PE - PE_{ref} = \iiint_{z_{ref}}^{surface} g[\rho(z) - 1027.4]z dz\, dA,$$
$$\tag{3}$$

where ~~z_1 and z_2~~z_{ref} represent the depth of the halocline ~~upper and~~lower boundary, and ~~ρ_{ref}~~A is ~~potential density at the base of~~ the ~~halocline.~~gyre area (Armitage et al., 2020; Bertosio et al., 2022; Polyakov et al., 2018).

175 Furthermore, ~~for discerning~~to discern the critical role of mesoscale eddies in balancing the halocline, we consider that the eddy advection velocity in the (y, z) plane can be defined from an eddy ~~streamfunction~~stream function ψ^* as

$$v^* = -\psi_z^*, w^* = \psi_y^* \tag{4}$$

and ψ^* is represented as ~~(Manucharyan et al., 2016; Manucharyan and Spall, 2016; Manucharyan and Isachsen, 2019)~~

$$\psi^* = \frac{\overline{V'S'}}{\overline{S_z}} = -\frac{\overline{w'S'}}{\overline{S_y}} \tag{5}$$

180 where $\overline{V'S'}$ is the average meridional eddy salt flux and $\overline{S_z}$ is the average vertical salt gradient (Manucharyan et al., 2016; Manucharyan and Spall, 2016; Manucharyan and Isachsen, 2019; Marshall and Radko, 2003). Here, bars and primes

correspond to ~~annul~~the annual mean and perturbation variables. ~~Due to~~Because buoyancy is mainly controlled by salinity in the Arctic, ψ^* represents the cumulative effects of eddy thickness fluxes that arise from correlations between eddy velocities and eddy- induced isopycnal displacements. Overall, when the vertical salt gradient is generally negative in the CB, a positive value of ~~Ψ*~~ψ^* indicates ~~a southward (northward) transportation~~southwards (northwards) transportations of ~~high~~(low) salinity (high-salinity) water and vice versa.

If eddy genesis is related to baroclinic instability, the baroclinic growth rate ω is correlated with EKE. The baroclinic growth rate ω can be estimated here by ~~(Simth, 2007)~~

$$\omega = f \sqrt{\frac{1}{6H} \int_{H}^{0} \frac{dz}{R_i(z)}} \tag{6}$$

where $R_i = N^2/[\left(\frac{\partial u}{\partial z}\right)^2 + \left(\frac{\partial v}{\partial z}\right)^2]$ is the Richardson number~~.~~ (Smith, 2007). We call the inverse of this quantity ω^{-1}=T the "Eady timescale". The Eady timescale should be short where there is anomalously high EKE or weak stratification.

3 BG halocline variability

~~This~~In this section ~~is aimed~~, we aim to investigate the ~~spatio-temporal~~spatiotemporal variability ~~of~~in the halocline in the BG region, particularly its varying asymmetry inside, which is the ~~main~~focus of this article. The halocline's depth, thickness and strength, and vertical structure are ~~detailedly analyzed~~analysed in detail below, all of which indicate its meridional asymmetry ~~at the mean time~~.

3.1 Temporal variation ~~of~~in the halocline

~~Under~~With the spin-up of the BG, the isopycnals of the PWW layer in the cold halocline have deepened (Kenigson et al., 2021). We ~~have chosen~~chose the ~~special~~25 and 27.4 isopycnal ~~surfaces~~surfaces to characterize the halocline top and base ~~of the halocline.~~. Figure ~~2a and b show~~2 shows the discontinuous variation ~~of~~in the halocline upper/lower boundary and thickness at four moorings from MMP. ~~As a whole,~~To supply the lack of MMP measurements, the annual means of halocline depth and thickness are also analysed based on CTD. Compared with MMP results, the mean relative errors of CTD on halocline depth (thickness) are 2.0% (3.4%), 4.4% (7.0%), and 1.0% (3.0%) for moorings A, B, and D, respectively. Given that the rangeability of the halocline top is much smaller than that of the halocline base, and the depth of the halocline upper/lower boundary at a single mooring shows ~~basically~~consistent trends, ~~so~~we mainly focus on the variation ~~of~~in halocline base ~~depth. But there~~. There are different characteristics of variation during 2003–2018 despite a lack of ~~void~~measurements ~~in~~over time. ~~Finite~~The finite MMP results at mooring C ~~show that~~showed an increasing trend ~~of~~in the depth and thickness of the halocline before 2008~~. Besides~~, well overlapped with mooring B. In addition, other moorings provided results over a longer term, which captured a deepening of the halocline base and an ~~increasing of~~increase in thickness over the years from 2003 to 2018. The thickness of the halocline at mooring B ~~located~~in the northwestern part of CB increased steadily by ~~about~~approximately 70

m~~, at the same time~~; moreover, the depth of the halocline base deepened by up to 70 m over the years 2003–2018. The thickness of the halocline in the southern part of the basin (moorings A and D) ~~both~~ increased by ~~about~~approximately 30 m ~~company~~ with the halocline base deepening by approximately 40 m. ~~It's worth noting that~~Notably, the depth of the halocline ~~has~~had a stagnant phase and even ~~opposite~~decreasing development over the years between 2003–2007 and 2015–2018. ~~Particularly,~~ ~~linear~~Linear trends and mean values of the halocline depth and thickness in three periods (2003–2007; 2008–2014; 2015–2018) are computed (Table 1). A negative trend of halocline depth is ~~clearly~~clear during 2008–2014 in the southern sites of the basin (moorings A and D), but the former and latter periods both mostly exhibit positive trends in halocline depth and thickness. The ~~variation~~variations at ~~the only~~ northern ~~site (mooring~~sites (moorings B and C) covering three periods ~~shows~~are similar, which show entirely different features~~, the~~ from southern sites. The halocline thickness reveals a negative trend in the third period (after ~~2015) that eventually remains a steady level~~2014) while the halocline depth ~~of that still keeps on~~continues deepening~~.~~ ~~In final,~~ over the whole period. The halocline thickness and depth ~~at~~between every site ~~tends~~tend to be ~~homogeneously~~ ~~distributed and the~~at a nearly identical level in the final period and those differences are ~~obviously shrunken~~smaller than ~~before~~in the first period.
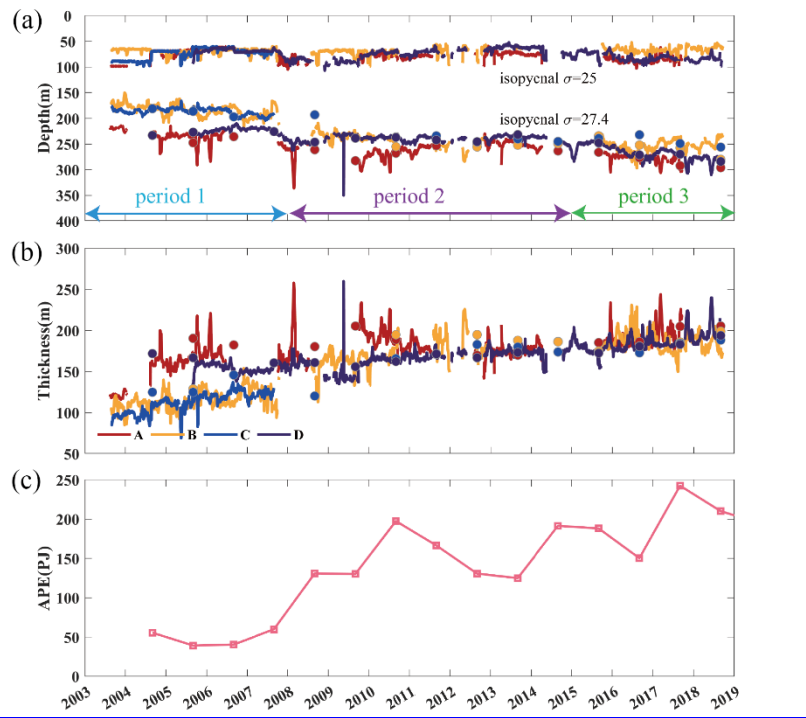
Figure 2. Time series of (a) depth of isopycnals 25 kg/m³ (upper coloured lines) and 27.~~4kg~~4 kg/m³ (upper coloured lines) representing the top and base of the halocline, and (b) halocline thickness between isopycnals 25 kg/m³ and 27.4 kg/m³ ~~and (c) APE~~ for moorings A, B, C, and D during 2003–2018. (c) Annual means of APE in the BG box calculated from CTD. Note that the ~~abnormal values~~anomalies record eddies were existent at that time. Coloured dots indicate the annual means near the four moorings derived from CTD.

APE, a good integral indicator of changes in overall halocline strength in the ~~CB~~BG box, is also computed here by Eq. ~~(4).~~(3) using CTD surveys. As ~~is~~ shown in Fig. 2c, ~~the variation is similar with that of halocline thickness. Initially~~there was a continuous increase before 2009. However, APE ~~revealed a striking difference between the northern (moorings B and C) and southern sites (moorings A and D) around the basin. The trend of APE showed a weak~~was continuously decreasing ~~after 2008 and then recovered to some extent at~~ in 2010–2014, implying a flattening of isopycnals in the ~~southern moorings. In contrast, APE at the northern moorings kept on improving until 2014 and then the growth stagnates. The difference among moorings reduced in final, and APE all~~ BG. There has not been an obvious trend since 2015 but remained ~~about 3×10⁵ J/m², that was the maximum value over the years.~~at a relatively stable level. We infer the ~~variability of~~variabilities in the halocline and APE have a relationship with the BG spin-up and the largest ~~increasing of~~increase in FWC during 2003–2007 (Giles et al., 2012; Krishfield et al., 2014; Timmermans and Toole, 2023). ~~And then partial variables~~Halocline depth and thickness exist stagnant in the post spin-up term during 2008–2014 (Regan et al., 2020).

Table 1. Trends (~~whthin~~within the brackets, unit: m/yr) that all pass significant tests (confidence level 99%) and mean values (outside the brackets, unit: m) of the halocline~~'s~~ top, base, and thickness in three periods for moorings A, B, C, and D~~, respectively~~.

Moorings		Periods 2003–2007	2008–2014	2015–2018
	top	75.4(-2.7)	77.8(-2.0)	86.2(-1.2)
A	base	236.4(7.3)	261.1(-4.5)	278.1(7.9)
	thickness	161.0(10.0)	183.3(-2.5)	191.9(9.1)
	top	69.1(0.5)	69.8(-2.0)	66.8(-1.1)
B	base	184.1(4.9)	241.1(5.4)	252.6(3.6)
	thickness	115.0(4.5)	171.3(7.3)	185.8(-2.4)
	top	74.3(-5.7)		
C	base	186.5(2.7)		
	thickness	112.3(8.5)		
	top	69.3(2.2)	73.6(-3.9)	81.5(3.1)
D	base	223.7(0.4)	239.4(-0.4)	267.6(8.9)
	thickness	154.4(-1.8)	165.9(3.6)	186.1(5.8)

3.2 Changes in the meridional asymmetry

The gyre in the CB is marked by pronounced asymmetry (Regan et al., 2019), with changing spatial distributions of the freshwater and ocean dynamic height. The isopycnal slope is steeper over the southern continental slope than in the northern basin (Fig. 1d), which is in line with previous research (Proshutinsky et al., 2019; Regan et al., 2019; Zhang et al., 2023). According to section 3.1, we find that the major differences in evolution only between the north and south of the basin are obvious, which is not completely identical to previous findings. Previous observations have revealed that isopycnals have deepened at different rates in the northwestern and southeastern parts of the basin during 2002–2016 (Zhong et al., 2019). Here, we find the meridional difference between north and south is more obvious. Therefore, we turn to the inhomogeneous gridded in situ hydrographic data from the latest CTD survey to obtain a better understanding of the overall asymmetrical halocline across the fundamental BG box (Fig 1.a). From the perspective of the horizontal maps in the three periods (Fig. 3) that are determined referring to the trends of halocline depth and thickness at the moorings, the horizontal patterns of the halocline depth show evident changes, implying the transformation of oceanic stratification in the upper layer. In the first period, the halocline base maps exhibit the significant difference between the north and south, and then, there is a gradual decline in the spatial difference as well as an overall deepening of the halocline. In the final period, the area with the maximum halocline depth is in the abyssal plain between the Canadian Arctic Archipelago and Northwind Ridge.
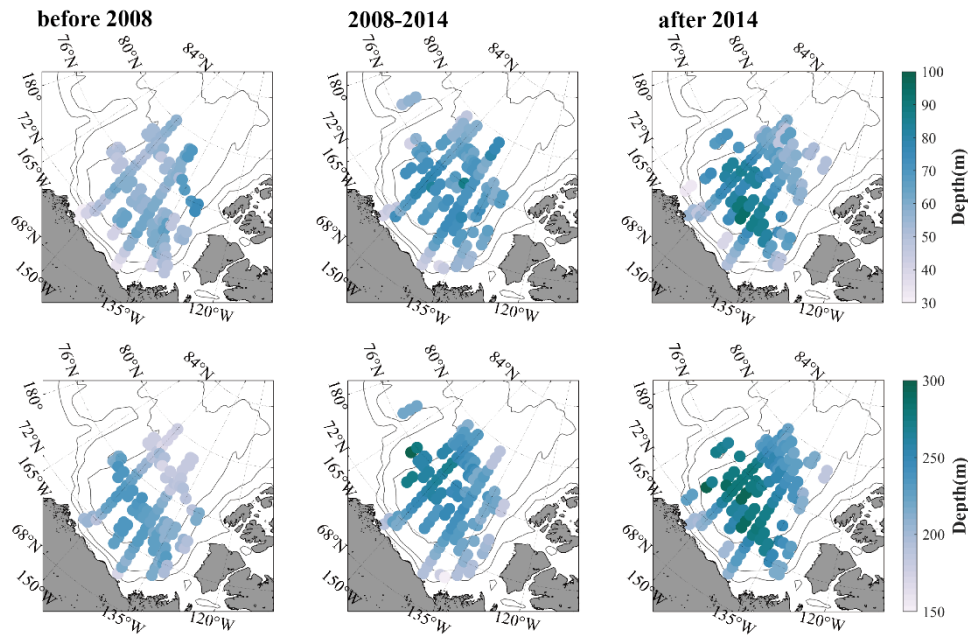
Figure 3. ~~(a-c)~~ Horizontal distribution of ~~depth of~~the halocline (upper panel) top and (lower panel) base across the ~~Canada~~
~~Basin~~Beaufort gyre region averaged in 2004–2007 (before 2008), 2008–2014, and 2015–2021 (after 2014~~), respectively. (d-e) As the~~
~~same with (a-c), but for APE in every period (integration between the top and base of halocline~~).

~~In addition, the~~According to the movements of the gyre centre mainly between 140°W and 150°W over 2003–2014 (Regan et
al. 2019), we select two north–south transects along 140°W and 150°W (Fig. 1b), which both traverse the deepest part of the
BG halocline (Fig. 1a), and make a comparison. The in situ hydrographic data are interpolated onto the regular grids to examine
the varying vertical structures of ~~halocline~~the isopycnals along the selected ~~transect (Fig. 1a). Notably,~~transects. We find that
the hydrographic structures ~~along 150°W and 140°W sections are~~from the two transects have similar features (Fig. 4), which
is the same as the former study (Timmermans and Toole, 2023). However, the change is more significant and the halocline
layer is much thicker along 150°W than along 140°W. Thus, we ~~only select a representative north–south transect mainly along~~
~~150°W to analyze here~~emphasise the shifts in halocline structures along the 150°W transect. The vertical distribution of the
isopycnal $\sigma = 27.4$ kg·m^{-3} surface show that it is shallowest ~ 200 m at the margins of the BG region and up to 80 m deeper in
the interior BG in the ~~later years~~final period (Fig. 4). Among the ~~early, median and later years shown~~three periods, the vertical
structures of isopycnals, especially the lower boundary of the halocline layer, reveal apparent changes between the marginal
and interior gyre. ~~From transects of potential density (Fig. 4), initially~~Initially, there was ~~an~~a distinct uplift of the halocline
~~towards~~heading to the ~~north~~northern edge of BG, with the depth of halocline base in the south (~74°N) ~~about 50~~approximately
30 m lower than in the north (~77°N). The difference between the north and ~~the~~ south was narrowed with isopycnals generally
deepening from the view of the average vertical structure during 2008–2014, and even the northern halocline ~~is~~was lower than
the southern district ~~(the difference is less than 10 m)~~. In the ~~third~~final period (after 2014), the ~~depth of the~~halocline ~~has~~depth

11

changed less in comparison with the previous periods~~, and~~. Additionally, the halocline ~~is clearly~~depth and thickness were meridionally ~~symmetric~~symmetrical, shaped like a horizontal bowl, ~~as if~~implying that it ~~has~~had reached a state of equilibrium. As ~~can be~~ seen from the spatial maps and vertical structures of the halocline ~~and APE~~, the characteristic of meridional asymmetry ~~was~~has been gradually weakening in ~~recent years.~~the final period. We infer there ~~is possibly existing~~are other physical ~~process join in~~processes contributing to the variability~~and we are plan to discuss below~~.
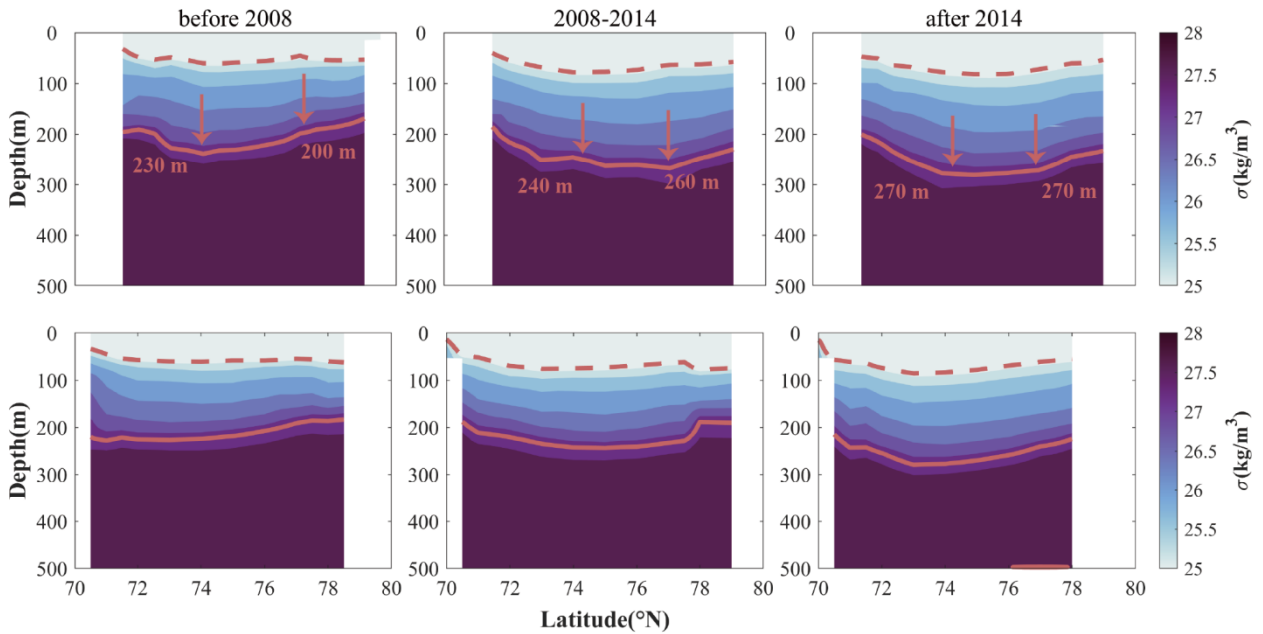
Figure 4. Vertical transects along (upper panel) 150°W and (lower panel) 140°W of interannual mean potential density using data from CTD measurements in 2004–2007 (before 2008), 2008–2014, and 2015–2021 (after 2014~~), respectively.~~). The dashed (solid) lines indicate the depth of σ = 25 (27.4) kg·m⁻³ representing the the halocline top (base~~)~~). The depths of halocline base on either side are marked in the upper panel.

4 ~~Spatio-temporal~~Spatiotemporal variability ~~of~~in eddy activity

As ~~was~~ revealed ~~by the former~~ in previous research, a regime shift of the BG occurred in 2007–08, with a spin-up phase of the gyre ~~occurred~~ from 2003 to 2007 and ~~a stabilization~~stabilisation after 2007 (Regan et al., 2020). ~~The depth, strength, core location of halocline all imply the shift of the gyre and FWC variability.~~ With BG spin-up and ~~environmental conditions changing~~regional sea ice retreat, mesoscale eddies are responding to dissipate extra energy input and influence the ~~potential~~ energy redistribution. ~~In this section the spatio-temporal variability of eddies by~~ (Armitage et al, 2020). It is speculated that the eddy ~~detection and EKE (a critical criterion to measure the strength of eddies) will be discussed.~~

~~4.1 Eddy~~ genesis is related to APE accumulation and release in the BG region, which can influence the vertical ~~distribution~~structure of the internal halocline (Manucharyan and Spall, 2016; Manucharyan et al., 2016). In the final period,

12

the developments of meridional asymmetry in the halocline layer and APE within the BG box have been inhibited. Under this background, the spatiotemporal variability in eddy activity, needed for a comprehensive understanding, is discussed in this section.

4.1 Eddy detection and variation

We ~~now~~ outline how mesoscale eddies can be detected based on moored observations. When eddies occur locally, there are strong horizontal velocities accompanied by isopycnal displacements. ~~As for~~For anticyclonic (cyclonic) eddies, the isopycnals are convex (concave). ~~By distinguishing the anormal~~We distinguish horizontal speeds larger than 10 cm/s and ~~the~~ isopycnal displacements, which are both ~~the~~ criterion used in the past ~~works~~literature (Timmermans et al., 2008; Zhao et al~~.,~~., 2014; Zhao and Timmermans, 2015~~), we counted the annual number of eddies in the upper layer (Fig. 5a).~~). In all, ~~there are~~ 37, 40, 7 and ~~43eddies~~ 43 eddies are detected above 500 m at ~~mooring~~moorings A~~-~~–D~~, respectively. They are mostly concentrated between the upper and lower halocline boundaries. As is the same with~~. Similar to previous works (e.g., Zhao et al., 2014; Zhao and Timmermans, 2015), in ~~the majority of~~ most instances, the ~~abnormal~~ temperature/salinity anomalies and convex isopycnal displacements in the eddy core are pervasive. ~~The all cold~~Cold-core eddies ~~are accounted~~account for 61.4%. ~~Most~~A total of ~~these~~98% of eddies are anticyclones and only ~~3~~three eddies detected at mooring C are cyclones. The cold-core anticyclones are ~~popular~~common in the BG region due to ~~oceanic stratification and~~ large-scale ~~dominated~~dominant anticyclonic circulation~~.~~ coupled with oceanic stratification, where cold and fresh Pacific water overlies warm and salty Atlantic water. Furthermore, for ~~the location of~~ mooring C, which is less controlled by the BG, with weaker mean flows (Fig. 1), the characteristics of eddies there ~~is~~are different from others. Some of the eddies are ~~cyclone~~cyclones that are seldom discovered at other moorings. ~~The~~Cyclone existence ~~of cyclones are~~is related to frontal instability near 80°~~ ~~N ~~that~~, which contributes ~~the eddy~~to cyclone formation (Manucharyan and Timmermans, 2013; Timmermans et al., 2008).

In addition, we confirm annual mean days of existing eddies and counts of warm-core and cold-core eddies over 500 m through moored observations. The interannual variations in days of recording mesoscale eddies and the counts of eddies are highly similar at moorings A and B, and several respective peaks are predominant (Fig. 5, days of effective observations exceed 200 days in most eddy-rich years). The days of eddy activities demonstrate considerable interannual fluctuations. Over the whole period, 2005, 2010, and 2017 for mooring A are eddy-rich years; for mooring B, 2005, 2009 and 2018 (144 days record valid observations) are eddy-rich years, which is affected by spatial inhomogeneity of eddy distribution or eddy transportation from the southern BG region (Armitage et al., 2020), the key area for eddy generation (Kubryakov et al., 2021; Manucharyan and Isachsen, 2019; Zhao et al., 2014). After 2014, eddy activities at mooring A (B) were more active than the medium period 2009–2014 (2010–2014) when there was a decreasing trend in eddy days. Despite the eddy days for mooring D showing a smaller fluctuation than other moorings, the amplitude of eddy number is noticeable. The in situ measurements at mooring D also capture a considerable amount of mesoscale eddies, with a decreasing trend in eddy number during the medium term 2009–2014 in line with other moorings.

13
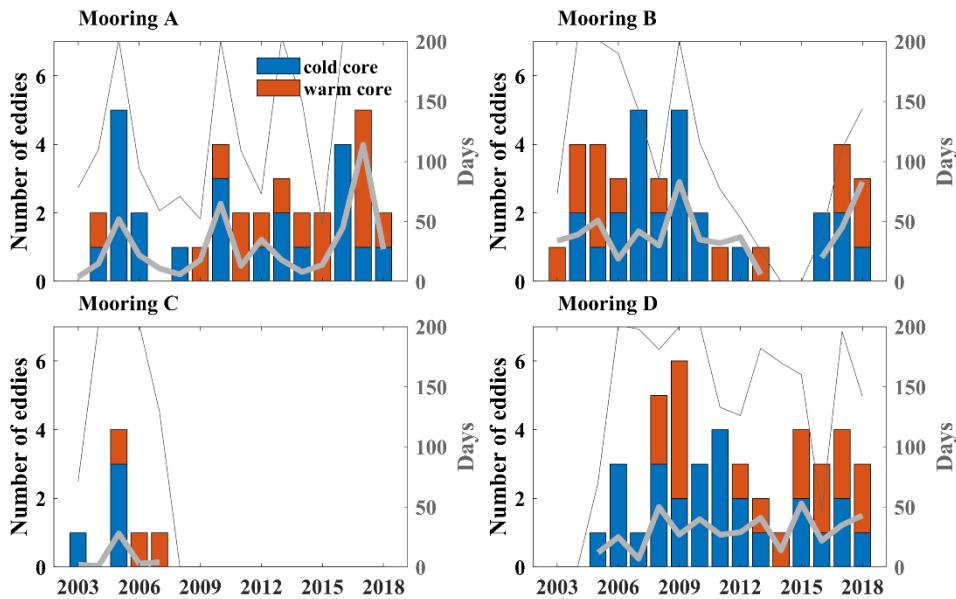
Figure 5. Interannual evolution of the days of existing eddies (thick grey line) and number of eddies (bar) for four moorings. The blue and red bars indicate the counts of cold-core and warm-core eddies, respectively. Thin grey lines signify the days of recording valid observations in every year.

Eddies are common between the upper and lower halocline boundaries (Fig. 6a). Additionally, comparing the vertical structures of EKE along with kinetic energy of individual eddies (KE_{eddy}) profiles in three periods at the moorings, we find thatKE_{eddy} accounts for ~ 50% of EKE (Fig. 6b). EKE changed, as a measurement for eddy strength, can well replicate the main feature of KE_{eddy} profiles. EKE changes significantly above the halocline in the three periods (Fig. 5b). The EKE, while below the halocline layer, it is relatively weaker than that in the upper layer, and its multiyear variation is much smaller. The vertical structures of EKE in the basin and its marginal seas can be classified into two types. The first type is that EKE is surface-intensified up to ~ 0.01 m^2/s^2 at the surface and it decays with depth. The second onetype is bimodal with separate comparably high values at the surface of less than 50 m and at the subsurface of approximately 90–250 m between the upper and lower halocline boundaries. In the first period, EKE above the BG halocline remained at a relatively low level, and it has increased in the second period when the BG circulation appeared to be stabilizing (Zhang et al., 2016).. The results from three moorings (all of them except mooring C are detected after 2008) showshowed that EKE was strengthened to varying degrees, accompanied by a deepening of the halocline lower boundary. At the southwestern corner (mooring A) of the basin,, only three eddies were detected in the first period. EKE increased in the second period when there were 15 eddies and remained stable in the third period; northwestern (with 13 eddies. Northwestern (mooring B) EKE strengthenedwas stronger with 14 eddies in the second period and weakenedthan before, despite 17 eddies detected in 2003–2007. EKE was weaker in the third period; southeastern (due to less valid observations. Southeastern (mooring D) subsurface EKE didn't occurdid not show

14

360 apparent growth until the third period due to much stronger eddies detected. There were only 14 eddies in 2014–2018 and 24 eddies detected in 2008–2014. In short, there were either stronger eddies or more eddies after 2014 than before.
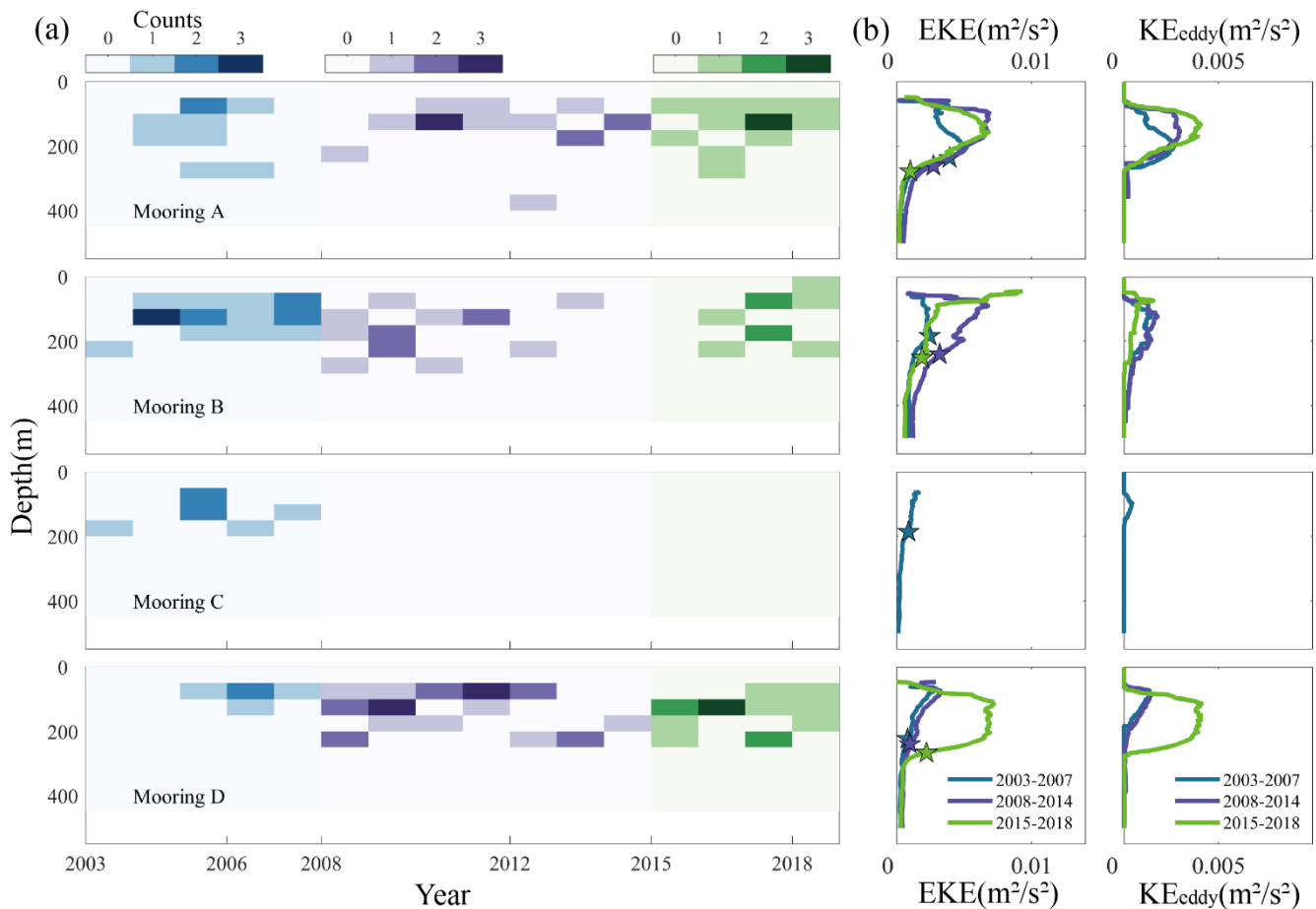
Figure ~~5~~6. (a) Hovmöller diagrams of depth against time showing annual ~~single~~ eddy counts in the upper layer at moorings A–D~~,~~
365 ~~respectively.~~. Blue, purple, and green shadings denote the spans of the three periods. (b) ~~Vertical~~Interannual mean vertical profiles
of ~~mean~~ eddy kinetic energy (EKE ~~for four moorings over years in the three periods.~~) and kinetic energy from eddies (KE$_{eddy}$).
Coloured stars indicate the depths of the halocline base in corresponding periods.

4.2 ~~Interannual~~Long-term EKE ~~patterns~~evolution from multiple datasets

The BG region, a focal area for mesoscale ~~phenomenon~~phenomena in ~~the~~ previous studies (Armitage et al., 2020; Regan et al.,
370 2020; Zhao and Timmermans, 2015; Zhao et al., 2016), mainly consists of a southern narrow continental shelf close to the
Alaska coast and a sizable deep basin. The Chukchi–Beaufort slope is the major sector for eddy generation by baroclinic
instability (Spall et al., 2008~~)~~), with a surface front approximately along the 300 m isobath (Timmermans and Toole, 2023),
and then eddies carrying ~~pacific~~Pacific water propagate to the central BG by the boundary current. Here, we focus on this area
to investigate the ~~variety of~~interannual mean surface EKE patterns from a broad perspective ~~used~~ by satellite–derived dynamic

15

375 heights. ~~Further, we seek for the main EKE patterns at surface in the three periods.~~ As ~~is~~ shown ~~(in~~ Fig. ~~6),~~7, the high-~~-~~value areas of EKE ~~is~~are mainly located along the continental slopes of the marginal CB especially the Alaska coast, mostly between ~~the~~ 1000 m and 3000 m isobaths. Indeed, energy is ~~the~~ strongest at the southwestern shelf break of CB near the Barrow Cape, which can ~~even~~ reach more than 5×10^{-3} m²/s², while it is even less than 1×10^{-3} m²/s² in the interior basin. Notably, the ~~horizonal~~horizontal pattern of EKE is not identical ~~with~~to that of mean kinetic energy (MKE) obtained by annual mean

380 geostrophic current (not shown here). ~~On the whole~~Overall, the area ~~where~~with the highest EKE is ~~strongest is~~ closer to the inshore shelf ~~sea side~~seas than the area ~~where~~with the highest MKE~~is strongest. EKE in~~. In every ~~term is all~~ period, EKE was significantly enhanced ~~comparing~~compared with that in the ~~former term~~previous period, and the strong EKE gradually developed from coasts to offshore regions and the central basin with time. For instance, from the interannual mean ~~horizonal~~horizontal patterns the region with the strongest EKE was mostly concentrated at the southern part of 72°N if we

385 only ~~notice~~noticed the section along the 1000 m isobath before 2007 (1993–2007) and it extended to ~~about~~approximately 73°N in the next period. Furthermore, the domain was even extended ~~northward~~northwards up to 74°N lying at the North Wind Ridge delineated by a long, clear, and curved ribbon in the ~~latest~~final period. We imply that eddy transportation contributes considerably to this development, which still ~~need more~~needs additional evidence.
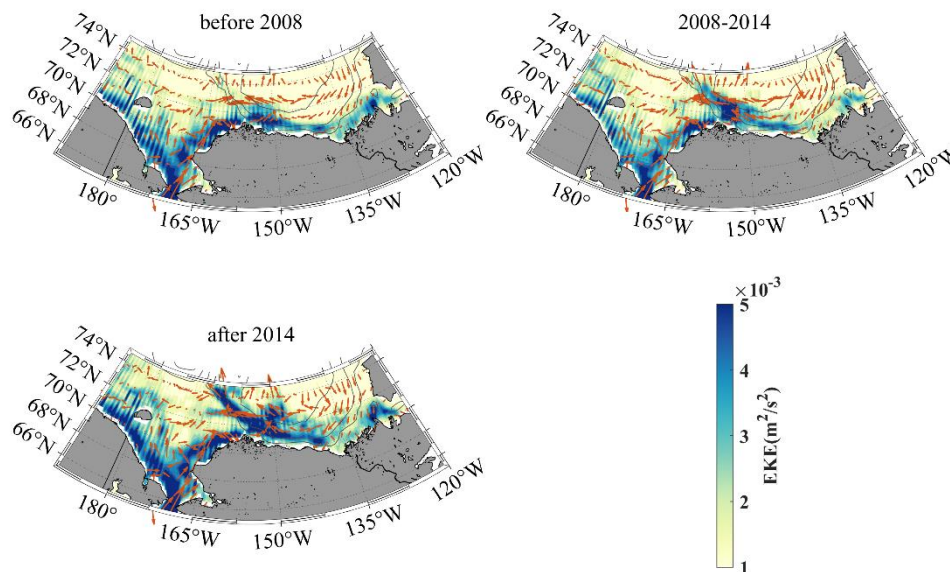
390

Figure ~~6~~7. Interannual mean maps of (shading) eddy kinetic energy (EKE) and (vector) geostrophic flows at the surface in 1993–2007 (before 2008), 2008–2014, and 2015–2019 (after 2014~~), respectively. ~~).

We confirmed the dates of existing eddies and annual number of warm or cold core eddies over 500 m through moored observations. The interannual variations in days of recording mesoscale eddies and the number of eddies are very similar at moorings A and B, and several respective peaks are predominant (Fig. 7, days of effective observations exceed 200 days in most eddy-rich years) in the three periods of revealing critical halocline changes discussed in section 3. In every dominating period of halocline variability there is one strong eddy-rich year coming to light under observation. Among them, 2005, 2010 and 2017 for mooring A are eddy-rich years; for mooring B, 2005, 2009 and 2018 (144 days record valid observations) are eddy-rich years. We can see that the days of eddy activities demonstrate considerable interannual fluctuations. It is speculated that the eddy genesis may be related to the accumulation and release of APE in the BG region and the transmeridional movements of BG, which modulates the vertical structure of internal halocline. Plus, the year with abundant mesoscale eddies at the northern site is more lagging about 1 year than that in the south latterly during medium term, which is affected by eddy transportation and spatial inhomogeneity. Therefore, in the latest term specially after 2007 enhanced eddy activity is noteworthy. Meanwhile, the amplitude of eddy activities at mooring D is obviously noticeable, although this site is far deviated from the Chukchi-Beaufort continental slope, which is2014). , The in situ measurement at mooring D captured a large number of mesoscale eddies, with a deceasing trend of number during medium term in line with the 2003-14 northwestern movement of the BG center (Regan et al., 2019). From 2017 onwards, the BG retreated from Mendeleev Ridge to the east (Moore et al. 2018) accompanied by elevated eddy activities.

NowadaysCurrently, the seasonality of EKE in the Arctic clearly now that it isis clear, generally maximalstronger in late summer or autumn and minimumweaker in spring or winter (Wang et al., 2020; Manucharyan and Thompson, 2022), which is similar withto other global regions (Rieck et al., 2015; Jia et al., 2011). Seasonal cycles of EKE in the central basin and basin boundary regions are both distinct (Fig. 8b). However, the researches about research on long-term EKE evolution areis still fewerlimited. The Alaska coast and the Chukchi–Beaufort Slope isare the key areaareas of varying EKE. Moreover (Fig. 7). In addition, we useduse finite data setsdatasets derived from SODA reanalysis, altimetry, and moored observations to explore the long-term variability ofin EKE between the central basin and continental slope. We selectedselect a western point of the Alaska coast called the AL region here near the Barrow Cape (Fig. 1b1c) and the BG region representing the central basin determined fromrepresented by the positions of four moorings. Here we think results of every mooring from MMPs are equally to characterAs shown in the eddy detection from MMP, eddies are common in the halocline layer. Results from MMP can well represent the variability in halocline eddies in the BG region, which are also consistent with former research. Results from every mooring are thought equal to characterize the main features of mesoscale processeseddy strength in the BG region, so the resultsEKE above the halocline base offor different moorings are vertically averaged with depth so as to obtain a longer continuous change of EKE the whole evolution over the years between 2003 and 2018.

The annual mean time series of surface EKE from SODA reanalysis (1980–2021) and altimetry (1993–2019) in the AL region and subsurface EKE from MMP (2003–2018) in the BG region are compared together (Fig. 8). In the AL region, surface EKE

was relatively weak ~~showing a slowly increasing over the years~~ before 2003, so we do not discuss it emphatically here. EKE ~~started to increase rapidly~~from altimetry has increased gradually since ~~2005~~the 1990s and peaked in 2009 ~~which lagged behind 1–2 years versus the variety of halocline and it indicated a decreasing until 2012 (AL).~~, and then, it decreased in 2009–2010, resulting in relatively weak and stable EKE in 2010–2015. Although the EKE from reanalysis is the highest estimate among

430   them, ~~but its fluctuation coincides with the results from altimetry~~it has also increased since the 1990s and remained at a stable level after 2010. In the BG region, subsurface EKE ~~started~~began to increase rapidly ~~about~~since ~~2007~~2003 and ~~also~~peaked in 2009~~.~~, and it indicated a ~~decreasing~~decrease until 2014, which was ~~a little~~slightly different from that in the AL~~. As a whole~~ region. Between 2010 and 2015, EKE ~~over the years between 2009 and 2014~~ was ~~both~~relatively weak and even decreased in the two regions ~~corresponding with~~, lagging behind the plateauing of halocline ~~variables.~~depth and thickness. These

435   characteristic shifts of eddy and oceanic stratification ~~evolution are~~were both ~~relative~~related to the varying physics of the gyre in the upper layer that ~~indicate~~indicated a strengthening during the years before 2007 and a possible ~~stabilization~~stabilisation since 2008 (Zhang et al., 2016). ~~Despite of~~After experiencing a low ebb, especially from altimetry and MMP, since 2014/2015, EKE has presented some enhancement ~~after experiencing low peaks, recently EKE has not exhibited rapid development on a long timescale but~~and oscillated around ~~a~~constant ~~level based on current data sets~~levels between the central ~~basin~~BG and its

440   marginal continental ~~slopes~~slope.
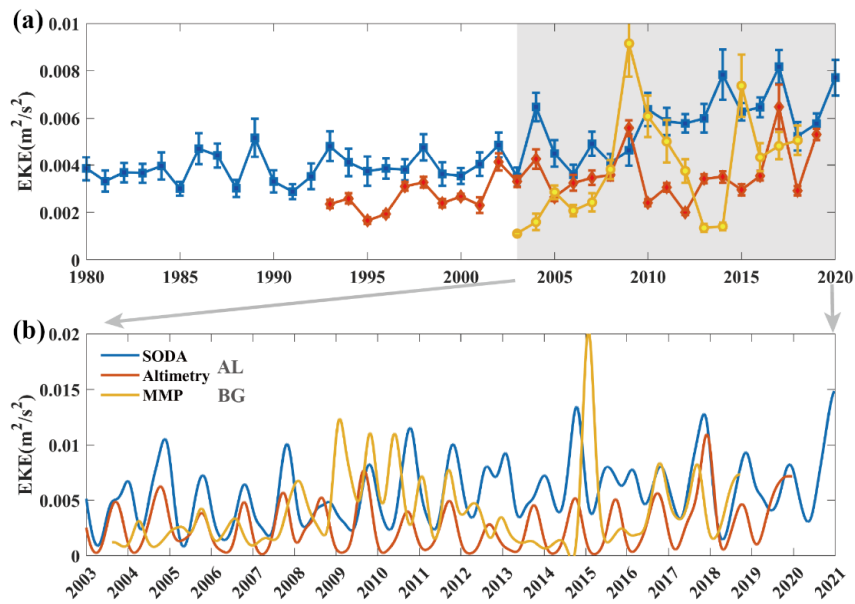
Figure 8. (a) Annual mean eddy kinetic energy (EKE) from MMP (2003–2018) averaged over 250 m in the BG region, altimetry (1993–2019~~)~~), and SODA (1980–2020) at the surface in the AL region. Error bars represent 1/10 standard deviation in every year.
445   **(b) Time series during 2003–2020 from partial results of (a), ~~that~~which are all smoothed by applying a 100--day low--pass filter.**

18

5 Eddy modulation in the asymmetrical halocline

In the context of gyre variability and the most prominent sea ice losses in the BG region (Timmermans and Toole, 2023), extra wind energy input leads to more active eddies. ~~The~~ Both surface and subsurface eddy activities are linked to gyre stability (Armitage et al, 2020; Manucharyan and Spall, 2016; Manucharyan et al., 2016). As discussed in sections 3 and 4, the halocline, as a measure of gyre stability, necessarily exhibits significant changes when ~~eddies generate and transport with flows~~ eddy number and strength are enhanced under this background. ~~However, in section 3~~ In particular, the variability of the halocline in the BG region demonstrates an apparent ~~reducing of~~ reduction in meridional asymmetry. How ~~do~~ eddies, as a key physical process ~~modulated,~~ modulate the halocline in this phenomenon? In this section, we ~~will~~ combine the variety of ~~eddies~~ eddy number and ~~EKE analyzed~~ strength analysed in ~~the~~ section 4 with the varying asymmetry of the halocline to ~~shed light on~~ elucidate how eddy ~~field modulates~~ activities modulate in the halocline.

5.1 Relationship between geostrophic currents and EKE

The APE and geostrophic currents are both diagnostic variables of the halocline depth (Armitage et al., 2020). Eddies are generated ~~through~~ by dissipating APE, and they gradually weaken the slope of isopycnals as well as geostrophic currents. Furthermore, the seasonality of eddy and geostrophic current fields is similar in the Arctic surrounding seas (Armitage et al., 2017). EKE at the southwestern ~~partner~~ part of the basin ~~where is~~ with the confluence of reversed zonal geostrophic currents is the strongest (Fig. 9). ~~And the~~ The area with stronger (weaker) zonal currents is ~~companying with~~ relatively weaker (stronger) EKE in the northern (southern) part of the Beaufort Sea slope (BSS) region. Along the Alaska coast (south of 72°N), EKE is higher ~~about 1~~ by approximately one order of magnitude than MKE ~~at most~~, indicating EKE is dominant in this region, while in the offshore deep basin, MKE is ~~even higher 1~~ one order of magnitude higher than EKE ~~that is agree~~, which agrees with most areas in the Arctic Ocean (von Appen et al., 2022). ~~Recently~~ After 2014, the domain with strong EKE has ~~been developing~~ gradually departed from coasts~~, such that EKE in partial areas specially central basin~~ (Fig. 7). Particularly, EKE has exceeded MKE ~~(not shown here).~~ near the central BG, representing the interior MKE was constrained.

19
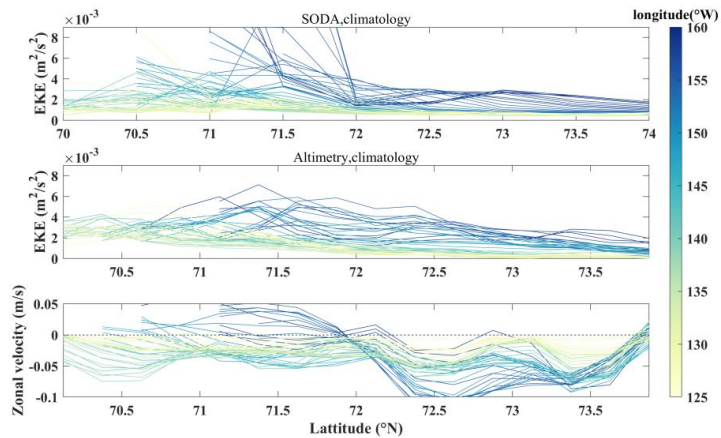
Figure 9. Climatology meridional eddy kinetic energy (EKE) from (upper panel) SODA reanalysis (1980–2020) and (middle panel) altimetry (1993–2019) in the Beaufort Sea slope (BSS) region. (lower panel) ~~As~~is the same ~~with~~as (a) and (b)~~)~~,~~)~~ but for climatology zonal geostrophic velocity.

We compare the probability analysis results of EKE and geostrophic velocities averaged in the AL region ~~(Fig. 1b)~~ based on the satellite altimetry ~~for~~in three periods ~~corresponding to~~(Fig. 10), which is estimated by statistical frequency of the ~~halocline change. From Fig. 10,~~area mean time series in every period. The annual mean EKE was significantly intensified by 17% (26%) from period 1 to period 2 (from period 2 to period 3~~), simultaneously~~). Furthermore, its main values within the extent with a probability of 68.4% were also enhanced. Although the velocities were both increased in the last two ~~terms~~periods, the magnitudes of their ~~increasing are~~increases were only 15% and 7%, which are much smaller than that of EKE. When the EKE in this region ~~remained a sharp increasing~~continued to sharply increase in the past, the velocity field ~~was increasing~~increased more slowly. The rate of velocity change ~~has begun~~began to decrease ~~in recent years~~, while EKE was still increasing rapidly, ~~implying~~representing that the difference between them ~~was~~has been magnified in recent years. For further ~~information~~clarification, we explore the relationship between these two variables. ~~Besides that~~In addition, we find that these variabilities ~~indicate~~show a strong correlation over the area of ~~we~~ interest (Fig. 10g). The correlation coefficients between EKE and local geostrophic velocities are mainly negative near the Alaska coast and partial central basin, which is verified by their variation in the AL region ~~while~~. However, the major correlation coefficients passing ~~a test of~~ the significance test level ~~of~~ 95% remain highly positive between the 1000 m and 3000 m isobaths along the southwestern margins of the basin, which is likely ~~to be~~ caused by the continuously enhanced EKE offshore even emerging in the deep basin.
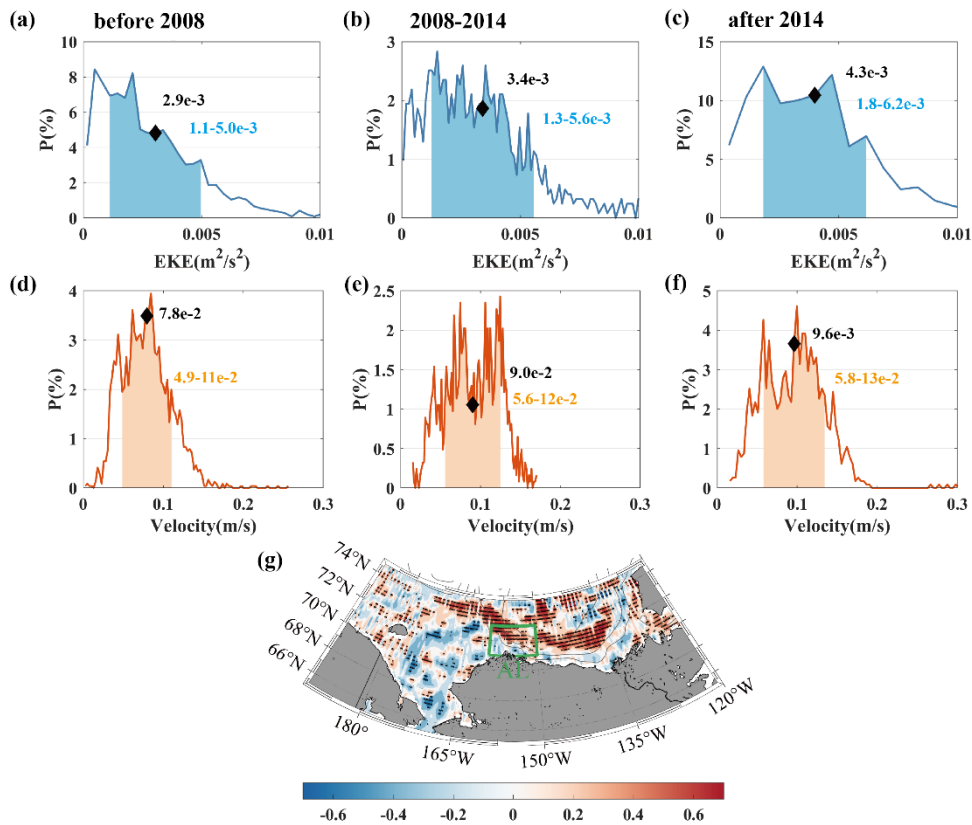
20

Figure 10. Probability of (a–c) eddy kinetic energy (EKE) and (d–e) geostrophic velocity in the Alaskan coast (AL) region during (a, d) 1993–2007, (b, e) 2008–2014, and (c, f) 2015–2019. Black diamonds represent mean values in three periods. The range of shading ~~means~~indicates the extent with a probability of 68.4%. (g) A map of the correlation coefficients between the annual mean eddy kinetic energy (EKE) and local geostrophic velocities in 1993–2019. Black dots indicate all positions that passed a ~~significant~~significance test (confidence level 95%).

5.2 Eddy lateral flux: a critical role in modulating the halocline

~~During 2009–2011 EKE~~In recent years, after APE continuously decreased during 2010–2014, EKE has remained at a relatively strong level compared with the mean value over the whole period. ~~At~~In the ~~same time~~meantime, the meridional asymmetry of the halocline geometry ~~has been~~was reduced, and the increasing rate of geostrophic currents ~~has been~~ slowed down. It is ~~known~~ currently known that eddies can not only dissipate APE but also hinder ~~the~~freshwater accumulation ~~of freshwater~~. As ~~is~~ discussed in section 3, the halocline vertical structure ~~tends~~has tended to be meridionally symmetrical in the BG region in recent years, which ~~is proved~~was proven by ~~in situ observation from~~ MMP and CTD observations. Here, we also find that this varying structure can be well replicated ~~schematically~~through SODA reanalysis schematically (Fig. 11a), although the results from SODA overestimate the depth of the halocline to a certain extent with an error of 30–40 m near the central basin. The changes ~~of~~in the halocline structure ~~and depth~~ at each side in the three periods obtained from SODA showed a strong

21

505　consistency with the results from the CTD, which is verified that the northern halocline was upperhigher than the southern part

before 2008 and then the halocline at each side along the meridional transect remained at a similar level after 2014.
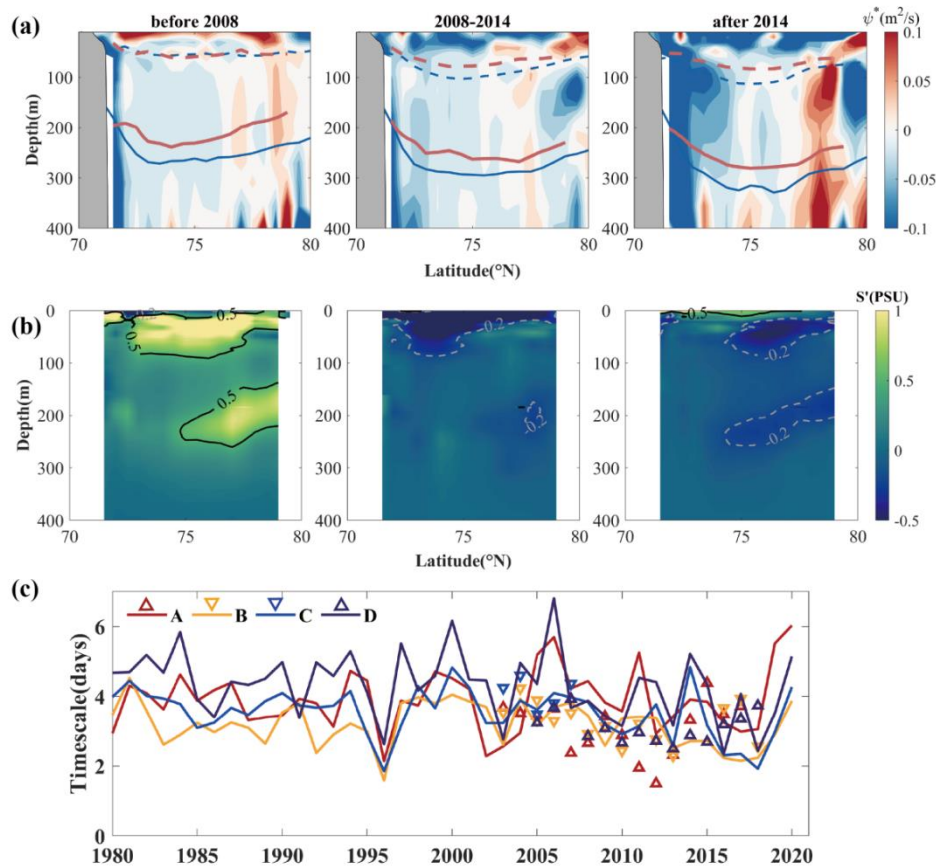
Figure 11. Transects of (a) eddy ~~streamfunction (unit: m²/s)~~stream function and (b) ~~abnormal~~ salinity ~~(unit: PSU)~~anomaly relative to the whole term averaged in 2004–2007 (before 2008), 2008–2014 and 2015–2020/2021 (after 2014), ~~that are~~ calculated from SODA
510　simulated now ~~till~~until 2020 and CTD observed ~~till~~until 2021~~, respectively~~. The dashed (solid) lines indicate the processed annual mean depth of isopycnal surface σ = 25 (27.4) kg·m⁻³ representing the halocline top (base) ~~of halocline~~ from SODA (~~bule~~blue lines, selected data are from September to October, which is mostly consistent with the observed data for CTD deployment) and CTD (red lines) during three periods. (c) Annual mean time series of the Eady timescale calculated from SODA (solid line) and MMP (triangle) at four moorings.

515　~~Aiming to explore what a critical role did eddies paly in the halocline, we analyze the eddy streamfunction evaluated by Eq.~~

~~(5) over a long-term scale based on SODA. As is shown (Fig. 11b), in the first period when the Eady timescale was relatively~~

~~large over the long term, the abnormal salinity in the mixed layer and the halocline was both positive. Combined with the~~

~~distribution pattern of eddy streamfunction, the eddy thickness flux was positive at surface due to the southward propagation~~

~~of low-salinity water, and above the base of the halocline was mainly distributed at the edge of the gyre. Low-salinity water at~~
520　~~subsurface in the south near the continental slope spread northward but in the north close to the deep basin it spread southward,~~

~~which formed a central converging pattern, so finally resulting in southern halocline much lower than the north at that time.~~

~~In the second period when a transformation appeared in the upper layer, the Eady timescale was decreasing meaning the~~

22

~~enhanced baroclinic instability in the BG. The mixing layer showed a low salinity anomaly and the pattern of eddy thickness flux indicated a northward propagation of low-salinity water. Meanwhile, there was an overall deepening of halocline depth.~~

525 ~~In the third period, significant low salinity anomaly in the halocline has been transferred from surface to subsurface. Besides, the main spatial pattern of eddy flux in this period was extremely similar to that in the former period with obviously strengthened. The low brine transmission caused by eddies replenished the surface freshwater in the north. Above the halocline, in the main range of 71° 79°N surrounding the central gyre, the convergence of anormal low-salinity was extremely strong. As a whole, the freshwater redistribution induced by these transportations due to eddy lateral flux are contributing to~~

530 ~~significantly diminished the meridional asymmetry of the halocline. Some of the low salinity water continues to spread northward, which is coinciding with the northward expansion of the gyre mentioned in a recent study (Bertosio et al., 2022).~~

Aiming to explore the critical role that eddies play in the halocline, we analyse the eddy stream function evaluated by Eq. (5) over a long-term scale based on SODA. In the first period, when the Eady timescale was relatively larger over the long term (Fig. 11c), meaning stronger stability, the salinity anomalies in the mixed layer and the halocline layer were both positive,

535 more than 0.5 (Fig. 11b). Combined with the distribution pattern of the eddy stream function, the eddy thickness fluxes were generally positive at the surface, about 0.1 m^2/s^2, and represented the southwards (northwards) propagation of low-salinity (high-salinity) water. However, in the halocline layer, stronger eddy fluxes were mainly distributed at the southern and northern edges of the gyre, finally resulting in a northern high-salinity anomaly and southern halocline much lower than the north at the same time. In the second period, when a transformation took place in the upper layer, the Eady timescale decreased, indicating

540 the enhanced baroclinic instability in the BG. There were low-salinity anomalies of less than -0.5 in the mixing layer, and eddy thickness fluxes of less than -0.1 m^2/s^2 indicated a northwards propagation of low-salinity water. In the meantime, there was an overall deepening of the halocline depth. In the third period, significantly low-salinity anomalies in the halocline were transferred from the surface to the subsurface. In addition, the main spatial pattern of eddy flux in this period was extremely similar to that in the former period but with obvious strengthening. In the mixing layer, the eddy thickness fluxes were less

545 than -0.2 m^2/s^2. The eddy-induced low-salinity water transportations replenished the freshwater in the north. In the halocline layer, among 71–79°N surrounding the gyre centre, the convergence of eddy lateral fluxes was extremely strong. Eddy fluxes were less than -0.1 m^2/s^2 on the southern edge and more than 0.1 m^2/s^2 on the northern edge, meaning that low-salinity water at the subsurface in the south near the continental slope spread northwards, but in the north it spread southwards, which formed a central-converging pattern. The freshwater redistribution induced by eddy lateral flux contributed to the significantly

550 diminished meridional asymmetry of the halocline. Some of the low-salinity water continued to spread northwards, which coincided with the northwards expansion of the gyre and freshwater release mentioned in a recent study (Bertosio et al., 2022).

6 Summary and discussion

~~The~~Our main objective ~~of this research~~ is to explore how long-term variations ~~of~~in eddy activity influence the ~~spatial-temporal~~spatiotemporal variability ~~of~~in the halocline under the BG system. In this study, our analyses of the halocline based

on in situ hydrologic data including MMP from moored observations and CTD under the BGEP project, both showed that the northern and southern ~~depth~~depths of isopycnals have deepened ~~in~~to different degrees in nearly the last ~~nearly~~ two decades. The halocline depth ~~and strength are both~~ significantly increased ~~among~~in the deep basin and continental slopes (Kenigson et al., 2021; Zhong et al., 2019). The halocline in the south ~~near 74°N has been~~ deepened by ~40 m, while that in the north ~~near 77°N has been~~ deepened by ~70 m over the years 2003–2018. After 2014, the difference ~~of~~in halocline depth at either side of the ~~two sides of the basin~~gyre was nearly negligible. The meridional asymmetry of the halocline with halocline depth lifting to the north was initially ~~was~~ shifted to a final nearly ~~symmetric~~symmetrical structure.

Furthermore, we investigated the ~~spatio-temporal~~spatiotemporal variability of eddies and EKE between the central gyre and continental slope to try to clarify why the halocline changed asymmetrically. There were 37, 40, 7, and 43 eddies detected in the upper layer at ~~mooring~~moorings A–D, 98% of which were anticyclones. The EKE at the southwestern corner was much stronger after 2008 than ~~that~~ in the previous period, but it remained relatively stable ~~latter~~later, which was consistent with the declined Eady timescale. ~~EKE above the halocline is intensified antecedently in the south compared with that in the north from mooring measurements, which is demonstrated by the long-term varying EKE distribution in the southwestern Arctic relating to the direction of eddy propagation from where they are generated.~~ With halocline depth ~~varying~~and variation, the number~~/~~ and strength of eddies at different sites as well as EKE at key regions ~~are exhibiting~~exhibit considerable interannual fluctuations ~~that are also related to the movements large-scale circulation.~~. There are more active and stronger eddies in the final period than before. The difference in eddy activity at each site is affected by spatial inhomogeneity of eddy distribution or eddy transportation from the southern BG region where they are generated. The highest EKE region is close to the reversal currents with relatively weaker mean flows there. When EKE is enhanced along the Chukchi/Beaufort continental slope ~~because of baroclinic instability~~, it ~~is~~ gradually ~~developed toward central basin~~develops towards the abyssal plain, which ~~is agree~~agrees with its intensification in the interior gyre in the final period from observations. ~~because of increased baroclinic instability and APE release.~~ Under ~~the~~increased eddy modulation ~~of continuously increasing EKE~~ provided by multiple ~~data sets~~datasets in the ~~key~~BG region ~~before 2009~~, the halocline depth experienced a deepening and then a lifting or ~~a~~ stagnate phase in the BG region, and the ~~increasing of~~increase in geostrophic flows also slowed down. ~~It is worth noting that~~Notably, the high EKE region ~~is~~was close to the reversal currents with relatively weak flows there.
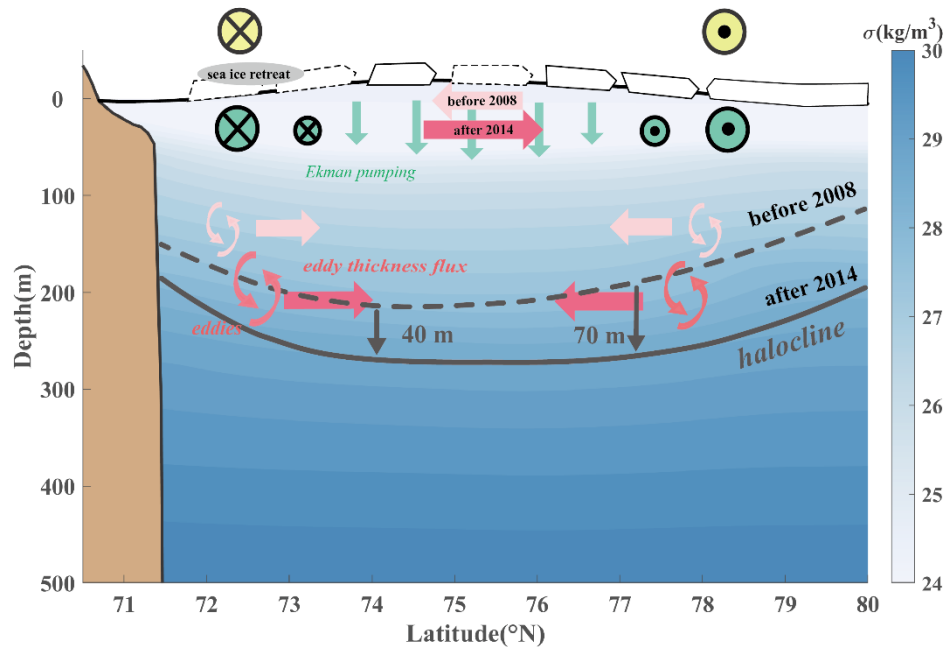
Figure 12. ~~Schematic~~The schematic **diagram under the BG system referred to the transect of 150°W, indicating the recent eddy modulation in the halocline. Shading is the climatology potential density from ~~2005–2017~~1990–2020 WOA climatology. Light (Dark) green arrows represent the eddy thickness momentum before 2008 (after 2014).**

Overall, the credible results revealed that the eddy ~~flux~~fluxes, playing a critical role in modulating the halocline, ~~has~~have adjusted the vertical structure of the halocline ~~through~~by affecting the freshwater redistribution in the past years comparing the initial period with the ~~latest~~final period (Fig. 12). ~~At the moment~~Currently, meridional asymmetry of the BG halocline ~~of the BG~~is distinctly diminished ~~attributing~~due to strengthened modulation of the eddy lateral flux. ~~At~~For the first ~~time~~period, the eddy ~~flux was~~fluxes were mostly positive above the mixed layer ~~meaning~~, indicating the ~~southward~~southwards propagation of ~~low-salinity water~~freshwater, which ~~explain~~explained the tilted structure of the halocline. In the ~~latest~~final period, the eddy ~~flux~~fluxes above the mixed layer ~~was~~were remarkably negative ~~meaning~~, indicating the ~~northward propagation~~northwards transportations of freshwater, and it formed an extremely strong convergent ~~center~~centre in the halocline layer. A series of processes promoted the surface low-salinity water ~~transmit~~transportations to the ~~northern basin~~north and it can be beneficial for ~~the~~freshwater confluence ~~of freshwater~~in the halocline at depth from two sides, which adjusted the meridional distribution of the halocline from asymmetry to relative symmetry.

To date, previous ~~researches hypothesized~~research hypothesised that the accumulation of freshwater driven by Ekman pumping is balanced by the ~~rectified~~effect of mesoscale eddies for ~~stabilizing~~stabilising the circulation (e.g., Davis et al., 2014; Manucharyan and Spall, 2016), not yet probing too much of the ~~eddy dynamics for modifying~~spatial difference in the halocline ~~asymmetry~~structure. This paper provides a possible perspective for understanding the long-term changes ~~of~~in the stratification structure and eddy field in the BG and the relationship between them. We expect it ~~can improve~~to further the knowledge of

large-scale circulation and mesoscale ~~process~~processes under the background of rapid changes in the Arctic. It is still necessary ~~for us~~ to ~~apply for~~use high--resolution ~~simulation and~~simulations combined with observations across the gyre to obtain a comprehensive understanding of interior ~~variation among~~variations between different physical processes ~~applying to promote~~, for promoting scientific development in ~~the~~ BG dynamics.

605 **Data availability**

Author contribution

LD provided the initial scientific idea and financial supports. LD and JL together conceived the idea for the present study. JL
615 and ST collected all available datasets. JL processed the data, plotted the results, and wrote the first version of the manuscript. All authors reviewed and edited the manuscript to its final version.

Competing interests

The authors declare that they have no conflicts of interest.

References

Aagaard, K., Coachman, L. K., and Carmack, E.: On the halocline of the Arctic Ocean. Deep-sea Res., 28, 529-545. https://doi.org/10.1016/0198-0149(81)90115-1,1981.

Armitage, T. W. K., Bacon, S., Ridout, A. L., Petty, A. A., Wolbach, S., and Tsamados, M.: Arctic Ocean surface geostrophic circulation 2003-2014, Cryosphere, 11, 1767-1780. https://doi.org/10.5194/tc-11-1767-2017, 2017.

Armitage, T., Manucharyan, G. E., Petty, A. A., Kwok, R., and Thompson, A. F.: Enhanced eddy activity in the Beaufort Gyre in response to sea ice loss. Nat. Commun., 11, 1-8. https://doi.org/10.1038/s41467-020-14449-z, 2020.

Bertosio, C., Provost, C., Athanase, M., Sennéchael, N., Garric, G., Lellouche, J. M., Bricaud, C., Kim, J. H., Cho, K. H., and Park, T.: Changes in freshwater distribution and pathways in the Arctic Ocean since 2007 in the mercator ocean global operational system. J. Geophys. Res. Oceans, 127, e2021JC017701. https://doi.org/10.1029/2021JC017701, 2022.

Bourgain, P., and Gascard, J. C. : The Arctic Ocean halocline and its interannual variability from 1997 to 2008. Deep-sea Res., 58, 745-756. https://doi.org /10.1016/j.dsr.2011.05.001, 2011.

Chelton, D. B., Schlax, M. G., Samelson, R. M., and de Szoeke, R. A.: Global observations of large oceanic eddies. Geophys. Res. Lett., 34, L15606. https://doi.org/10.1029/2007GL030812, 2007.

Davis, P. E. D., Lique, C., and Johnson, H. L.: On the link between arctic sea ice decline and the freshwater content of the Beaufort Gyre: Insights from a simple process model. J. Clim., 27, 8170-8184. https://doi.org/10.1175/JCLI-D-14-00090.1, 2014.

Doddridge, E. W., Meneghello, G., Marshall, J., Scott, J., and Lique, C.: A Three-way balance in the Beaufort Gyre: The Ice-Ocean Governor, wind stress, and eddy diffusivity. J. Geophys. Res. Oceans, 124, 3107-3124. https://doi.org /10.1029/2018JC014897, 2019.

Fer, I., Bosse, A., Ferron, B., and Bouruet-Aubertot, P.: The dissipation of kinetic energy in the Lofoten Basin eddy. J. Phys. Oceanogr., 48, 1299-1316. https://doi.org/10.1175/JPO-D-17-0244.1, 2018.

Giles, K. A., Laxon, S. W., Ridout, A. L., Wingham, D. J., and Bacon, S.: Western Arctic Ocean freshwater storage increased by wind-driven spin-up of the Beaufort Gyre. Nat. Geosci., 5, 194-197. https://doi.org/10.1038/ngeo1379, 2012.

Huang, R. X.: Mixing and available potential energy in a Boussinesq ocean. J. Phys. Oceanogr., 28, 669-678. https://doi.org/10.1175/1520-0485(1998)028<0669:MAAPEI>2.0.CO;2, 1998.

Huang, J., Zhang, X., Zhang, Q., Lin, Y., Hao, M., Luo, Y., Zhao, Z., Yao, Y., Chen, X., Wang, L.,Nie, S.,Yin, Y., Xu, Y., and Zhang, J.: Recently amplified arctic warming has contributed to a continual global warming trend. Nat. Clim. Change., 7, 875-879. https://doi.org/10.1038/s41558-017-0056-y, 2018.

Jia, F., Wu, L., and Qiu, B.: Seasonal modulation of eddy kinetic energy and its formation mechanism in the southeast Indian Ocean. J. Geophys. Res. Oceans, 41, 657-665. https://doi.org/10.1175/2010JPO4436.1, 2011.

Kenigson, J. S., Gelderloos, R., and Manucharyan, G. E.: Vertical structure of the Beaufort Gyre halocline and the crucial role of the depth-dependent eddy diffusivity. J. Phys. Oceanogr., 51, 845-860. https://doi.org/10.1175/JPO-D-20-0077.1, 2021.

660   Kozlov, I. E., Artamonova, A. V., Manucharyan, G. E., and Kubryakov, A. A.: Eddies in the western Arctic Ocean from spaceborne SAR observations over open ocean and marginal ice zones. J. Geophys. Res. Oceans, 124, 6601-6616. https://doi.org/10.1029/2019JC015113, 2019.

Krishfield, R. A., Proshutinsky, A., Tateyama, K., Williams, W. J., Carmack, E. C., McLaughlin, F. A., and Timmermans, M. L.: Deterioration of perennial sea ice in the Beaufort Gyre from 2003 to 2012 and its impact on the oceanic freshwater
665   cycle. J. Geophys. Res. Oceans, 119, 1271-1305. https://doi.org/10.1002/2013JC008999, 2014.

Kubryakov, A. A., Kozlov, I. E., and Manucharyan, G. E.: Large mesoscale eddies in the western Arctic Ocean from Satellite altimetry measurements. J. Geophys. Res. Oceans, 126, e2020JC016670. https://doi.org/10.1029/2020JC016670, 2021.

Luecke, C. A., Arbic, B. K., Bassette, S. L., Richman, J. G., Shriver, J. F., Alford, M. H., Smedstad, O. M., Timko, P. G., Trossman, D. S., and Wallcraft, A. J.: The global mesoscale eddy available potential energy field in models and
670   observations. J. Geophys. Res. Oceans, 122, 9126-9143. https://doi.org/10.1002/2017JC013136, 2017.

Manley, T. O., and Hunkins, K.: Mesoscale eddies of the Arctic Ocean. J. Geophys. Res. Oceans, 90, 4911-4930. https://doi.org/10.1029/JC090iC03p04911,1985.

Manucharyan, G. E., and Timmermans, M.: Generation and separation of mesoscale eddies from surface ocean fronts. J. Phys. Oceanogr., 43, 2545-2562. https://doi.org/10.1175/JPO-D-13-094.1, 1985, 2013.

675   Manucharyan, G. E., and Spall, M. A.: Wind-driven freshwater buildup and release in the Beaufort Gyre constrained by mesoscale eddies. Geophys. Res. Lett., 43, 273-282. https://doi.org/10.1002/2015GL065957, 2016.

Manucharyan, G. E., Spall, M. A., and Thompson, A. F.: A theory of the wind-driven Beaufort Gyre variability. J. Phys. Oceanogr., 46, 3263-3278. https://doi.org/10.1175/JPO-D-16-0091.1, 2016.

Manucharyan, G. E., Thompson, A. F., and Spall, M. A.: Eddy memory mode of multidecadal variability in residual-mean
680   ocean circulations with application to the Beaufort Gyre. J. Phys. Oceanogr., 47, 855-866. https://doi.org/10.1175/JPO-D-16-0194.1, 2017.

Manucharyan, G. E., and Isachsen, P. E.: Critical role of continental slopes in halocline and eddy dynamics of the Ekman-driven Beaufort Gyre. J. Geophys. Res. Oceans, 124, 2679-2696. https://doi.org/10.1029/2018JC014624, 2019.

Manucharyan, G. E. and Stewart, A. L. (2022). Stirring of interior potential vorticity gradients as a formation mechanism for
685   large subsurface-intensified eddies in the Beaufort Gyre. J. Phys. Oceanogr., 52, 3349-3370, https://doi.org/10.1175/JPO-D-21-0040.1, 2022.

Manucharyan, G. E., and Thompson, A. F.: Heavy footprints of upper-ocean eddies on weakened Arctic sea ice in marginal ice zones. Nat. Commun., 13, 1-10. https://doi.org/10.1038/s41467-022-29663-0, 2022.

Marshall, J., and Radko, T.: Residual-mean solutions for the Antarctic Circumpolar Current and its associated overturning circulation. J. Phys. Oceanogr., 33, 2341-2354. https://doi.org/10.1175/1520-0485(2003)033<2341:RSFTAC>2.0.CO;2, 2003.

Meneghello, G., Marshall, J., Lique, C., Isachsen, P. E., Doddridge, E., Campin, J., Regan, H., and Talandier, C.: Genesis and decay of mesoscale baroclinic eddies in the seasonally ice-covered interior Arctic Ocean. J. Phys. Oceanogr., 51, 115-129. https://doi.org/10.1175/JPO-D-20-0054.1, 2021.

Moore, G. W. K., Schweiger, A., Zhang, J., and Steele, M.: Collapse of the 2017 winter Beaufort High: a response to thinning sea ice? Geophys. Res. Lett., 45, 2860-2869. https://doi.org/10.1002/2017GL076446, 2018.

Munk, W., and Wunsch, C.: Abyssal recipes II: Energetics of tidal and wind mixing. Deep-sea. Res. Pt. I, 45, 1977-2010. https://doi.org/10.1016/S0967-0637(98)00070-3, 1998.

Niederdrenk, A. L., and Notz, D.: Arctic sea ice in a 1.5°C warmer world. Geophys. Res. Lett., 45, 1963-1971. https://doi.org/10.1002/2017GL076159, 2018.

Penduff, T., Barnier, B., Dewar, W. K., and O'Brien, J. J.: Dynamical response of the oceanic eddy field to the North Atlantic Oscillation: a model-data comparison. J. Phys. Oceanogr., 34, 2615-2629. https://doi.org/10.1175/JPO2618.1, 2004.

Polyakov, I. V., Pnyushkov, A. V., and Carmack, E. C.: Stability of the Arctic halocline: a new indicator of Arctic climate change. Environ. Res. Lett., 13, 125008. https://doi.org/10.1088/1748-9326/aaec1e, 2018.

Proshutinsky, A., Krishfield, R., Timmermans, M., Toole, J., Carmack, E., McLaughlin, F., Williams, W. J., Zimmermann, S., Itoh, M., and Shimada, K.: Beaufort Gyre freshwater reservoir: State and variability from observations, J. Geophys. Res. Oceans, 114, C00A10, https://doi.org/10.1029/2008JC005104., 2009.

Proshutinsky, A., Krishfield, R., Toole, J. M., Timmermans, M. L., Williams, W., Zimmermann, S., Yamamoto Kawai, M., Armitage, T. W. K., Dukhovskoy, D., Golubeva, E., Manucharyan, G. E., Platov, G., Watanabe, E., Kikuchi, T., Nishino, S., Itoh, M., Kang, S. H., Cho, K. H., Tateyama, K., and Zhao, J.: Analysis of the Beaufort Gyre freshwater content in 2003-2018. J. Geophys. Res. Oceans, 124, 9658-9689. https:// doi.org/10.1029/2019JC015281, 2019.

Raj, R. P., Johannessen, J. A., Eldevik, T., Nilsen, J. E. O., and Halo, I.: Quantifying mesoscale eddies in the Lofoten Basin. J. Geophys. Res. Oceans, 121, 4503-4521. https://doi.org/10.1002/2016JC011637, 2016.

Regan, H. C., Lique, C., and Armitage, T. W. K. : The Beaufort Gyre extent, shape, and location between 2003 and 2014 from Satellite observations. J. Geophys. Res. Oceans, 124, 844-862. https://doi.org/10.1029/2018JC014379, 2019.

Regan, H., Lique, C., Talandier, C., and Meneghello, G.: Response of total and eddy kinetic energy to the recent spin-up of the Beaufort Gyre. J. Phys. Oceanogr., 50, 575-594. https://doi.org/10.1175/JPO-D-19-0234.1, 2020.

Rieck, J. K., Böning, C. W., Greatbatch, R. J., and Scheinert, M.: Seasonal variability of eddy kinetic energy in a global high-resolution ocean model. Geophys. Res. Lett., 42, 9379-9386. https://doi.org/10.1002/2015GL066152, 2015.

Rieck, J. K., Böning, C. W., and Greatbatch, R. J.: Decadal variability of eddy kinetic energy in the South Pacific Subtropical Countercurrent in an ocean general circulation model. J. Phys. Oceanogr., 48, 757-771. https://doi.org/10.1175/JPO-D-17-0173.1, 2018.

Serreze, M. C., and Barry, R. G.: Processes and impacts of Arctic amplification: A research synthesis. Global Planet. Change., 77, 85-96. https://doi.org/10.1016/ j.gloplacha.2011.03.004, 2011.

725 Shimada, K., Itoh, M., Nishino, S., McLaughlin, F., Carmack, E., and Proshutinsky, A.: Halocline structure in the Canada Basin of the Arctic Ocean. Geophys. Res. Lett., 32, L03605. https://doi.org/10.1029/2004GL021358, 2005.

Smith, K. S.: The geography of linear baroclinic instability in Earth's oceans. J. Mar. Res., 65, 655-683. https://doi.org/10.1357/002224007783649484, 2007.

Spall, M. A., Pickart, R. S., Fratantoni, P. S., and Plueddemann, A. J.: Western Arctic Shelfbreak eddies: Formation and 730 Transport. J. Phys. Oceanogr., 38, 1644-1668. https://doi.org/10.1175/2007JPO3829.1, 2008.

Stroeve, J., Holland, M. M., Meier, W., Scambos, T., and Serreze, M.: Arctic sea ice decline: Faster than forecast. Geophys. Res. Lett., 34, L9501. https://doi.org/10.1029/2007GL029703, 2007.

Stroeve, J. C., Markus, T., Boisvert, L., Miller, J., and Barrett, A.: Changes in Arctic melt season and implications for sea ice loss. Geophys. Res. Lett., 41, 1216-1225., 2014.

735 Timmermans, M. L., Toole, J., Proshutinsky, A., Krishfield, R., and Plueddemann, A.: Eddies in the Canada Basin, Arctic Ocean, observed from Ice-Tethered Profilers. J. Phys. Oceanogr., 38, 133-145. https://doi.org/10.1175/2007JPO3782.1, 2008.

Timmermans, M. L., and Marshall, J.: Understanding Arctic Ocean circulation: a review of ocean dynamics in a changing climate. J. Geophys. Res. Oceans, 125, e2018JC014378. https://doi.org/10.1002/2013GL058951, 2020.

740 Timmermans, M., and Toole, J. M.: The Arctic Ocean's Beaufort Gyre. Annu. Rev. Mar. Sci., 15. 223-248. https://doi.org/10.1146/annurev-marine-032122-012034, 2023.

von Storch, J. S., Eden, C., Fast, I., Haak, H., Hernández-Deckers, D., Maier-Reimer, E., Marotzke, J., and Stammer, D.. Eddies and the distribution of eddy kinetic energy in the Arctic Ocean. Oceanogr. https://doi.org/10.5670/oceanog.2022.122, 2022.

745 Wang, Q., Koldunov, N. V., Danilov, S., Sidorenko, D., Wekerle, C., Scholz, P., Bashmachnikov, I. L., and Jung, T.: Eddy kinetic energy in the Arctic Ocean from a global simulation with a 1-km Arctic. Geophys. Res. Lett., 47, e2020GL088550. https://doi.org/10.1029/2020GL088550, 2020.

Zhang, J., Steele, M., Runciman, K., Dewey, S., Morison, J., Lee, C., Rainville, L., Cole, S., Krishfield, R., Timmermans, M., and Toole, J.: The Beaufort Gyre intensification and stabilization: A model-observation synthesis, J. Geophys. Res. 750 Oceans, 121, 7933-7952. https://doi.org/10.1002/2016JC012196, 2016.

Zhang, J., Cheng, W., Steele, M., and Weijer, W.: Asymmetrically stratified Beaufort Gyre: mean state and response to decadal forcing. Geophys. Res. Lett., 50. e2022GL100457. https://doi.org/10.1029/2022GL100457, 2023.

Zhao, M., Timmermans, M., Cole, S., Krishfield, R., Proshutinsky, A., and Toole, J.: Characterizing the eddy field in the Arctic Ocean halocline. J. Geophys. Res. Oceans, 119, 8800-8817. https://doi.org/10.1002/2014JC010488, 2014.

755 Zhao, M., and Timmermans, M. L.: Vertical scales and dynamics of eddies in the Arctic Ocean's Canada Basin. J. Geophys. Res. Oceans, 120, 8195-8209. https://doi.org/10.1002/2015JC011251, 2015.

Zhao, M., Timmermans, M., Cole, S., Krishfield, R., and Toole, J.: Evolution of the eddy field in the Arctic Ocean's Canada Basin, 2005-2015. Geophys. Res. Lett., 43, 8106-8114. https://doi.org/10.1002/2016GL069671, 2016.

Zhao, M., Timmermans, M. L., Krishfield, R., and Manucharyan, G.: Partitioning of kinetic energy in the Arctic Ocean's Beaufort Gyre. J. Geophys. Res. Oceans, 123, 4806-4819. https://doi.org/10.1029/2018JC014037, 2018.

Zhong, W., Steele, M., Zhang, J., and Cole, S. T.: Circulation of Pacific Winter Water in the western Arctic Ocean. J. Geophys. Res. Oceans, 124, 863-881. https://doi.org/10.1029/2018JC014604, 2019.

760